Spring 2011

Installation and performance evaluation of coaxial cable sensors for crack and corrosion detection

Iana Muchaidze

Department:

INSTALLATION AND PERFORMANCE EVALUATION OF COAXIAL CABLE SENSORS FOR CRACK AND CORROSION DETECTION

by

IANA MUCHAIDZE

A THESIS

Presented to the Faculty of the Graduate School of the

MISSOURI UNIVERSITY OF SCIENCE AND TECHNOLOGY

In Partial Fulfillment of the Requirements for the Degree

MASTER OF SCIENCE IN CIVIL ENGINEERING

2011

Approved by

Genda Chen, Advisor
David Pommerenke
John Myers

ABSTRACT

Even under service loads, reinforced concrete (RC) structures can develop cracks that result in excessive deflection of the structures and provide passages for moisture to corrode steel reinforcement. It is thus critical to develop a simple, cost-effective tool for real-time crack monitoring and associated corrosion detection that may affect the engineering maintenance of RC structures. The objectives of this study include: (1) to develop a die-cut manufacturing process of coaxial cables with spiral outer conductors, (2) to quantify the sensing properties of a miniaturized topology-based crack sensor, (3) to investigate the effectiveness of various sensor installation procedures in RC applications, and (4) to detect the distribution of corrosion in steel reinforcement. A new manufacturing process was developed to fabricate spirally-wrapped, miniaturized coaxial cables in the order of mm in diameter. To understand their performance and sensitivity, eight miniaturized sensors were fabricated and placed in seven RC concrete members that were tested under three-point loading. Various grout materials were also investigated to compare their effects on sensor sensitivity. Test results indicated that the miniaturized, die-cut coaxial cable sensors are more uniform and more sensitive to cracks than their early versions since the new manufacturing process can refine the topology of their outer conductors. Like embedment, surface attachment of a coaxial cable on a RC member can be effective with appropriate bonding agents such as Sikagrout materials. Preliminary tests by submerging coaxial cables into 3% and 5% NaCl solutions demonstrated that cable sensors can indicate the breaching of small holes on their outer conductor as a result of corrosion, potentially providing a promising technology for distributed corrosion detection.

ACKNOWLEDGMENTS

Many people at the Missouri University of Science and Technology deserve a great deal of gratitude for their guidance and assistance throughout my research. Firstly, I would like to express my deepest gratitude to my advisor, Dr. Genda Chen, for giving me the opportunity to work on the interesting research, and for patiently guiding me throughout my graduate study in general and my research in particular. His guidance and support helped me to excel in my knowledge and professional skills.

I would like to acknowledge the technical assistance of Dr. David Pommerenke on the subject of electromagnetics, without whom it would be impossible to complete this thesis. Furthermore, I would like to thank Dr. John Myers for serving on my committee and providing insightful comments.

Additionally, I would like to acknowledge the contribution of all people that assisted me in various ways throughout this project. The experimental part of this research would not have been possible without the help of Jason Cox, Mike Lusher, Steve Gable, and Gary Abbot. I want to thank Joseph Bishop and Andrei Radchenko the students in Electrical Engineering for their assistance during testing, simulations and data processing.

Special thanks go to my husband, Giorgi, my daughter, Nina, my family, and all my friends who have always believed in me and gave me the strength to accomplish my goals.

TABLE OF CONTENTS

Page

LIST OF ILLUSTRATIONS

LIST OF TABLES

NOMENCLATURE

Symbol	Description
ρ	Reflection Coefficient
V^+/V^-	The Ratio of the El. Field Strength of the Reflected Wave to that of the Incident Wave.
Z_+	Characteristic Impedances of the Sensor/Coaxial Cable Before the Discontinuity
Z_-	Characteristic Impedances of the Sensor/Coaxial Cableat the Discontinuity
Z_0	Caracteristic Impedance of the Transmition Line
x	Distance to the discontinuity
v	The Propagation Velocity of the Signal Along the Sensing Line
ε	Dielectric Constant
μ	Permeability
R	Per Unit Length Resistance
G	Per Unit Length Conductance
L	Per Unit Length Inductance
$Lgap$	Gap Inductance
C	Per Unit Length Capacitance
$Zgap$	Gap Impedance
ΔV	The apparent reflected voltage measured by the TDR or VNA
t	Time required for the signal propagation forth and back from the discontinuity

1. INTRODUCTION

1.1. GENERAL

Reinforced concrete (RC) is a widely used construction material in civil engineering. Despite its reputation as a generally durable material, a RC structure often experiences cracks or premature failures even under service loads when exposed to harsh environmental conditions. The aging deterioration of a RC structure is typically accompanied by the development of micro crack networks. The hairline cracks allow the salt-saturated meteoric water to penetrate through RC members, leading to the initiation of rebar corrosion followed by a significant loss of reinforcement cross-sectional area. In this case, not only the serviceability of a structure is compromised, but also the integrity of the structure may change as corrosion-induced stress continues to build up, resulting in premature collapse of the entire structure. Even if the presence of extensive cracking is tolerable from an engineering safety prospective, it often makes the public to lose confidence in the functionality of a structure. Therefore, it is of high importance to detect the initiation of a crack and monitor its continuing growth.

Availability of a reliable Structural Health Monitoring (SHM) technology that is capable of performing high quality structural assessment and delivers this information to an engineering community at a desirable time is imperative. It is envisioned that with such techniques the weakened zones of structural elements (such as bridge decks, columns act.) can be detected at the earliest stages of structural deterioration. Thus the corresponding remediation and retrofit means can be applied to an in-service structure at a minimum financial cost. Moreover, the threat to the human lives caused by unexpected and catastrophic structural failures can be minimized drastically.

During the past decade, strenuous attempts were made by an engineering community to develop various strategies and tools in SHM. Currently most efforts were limited to the applications of discrete transducers, such as strain gauges and accelerometers, and the use of nondestructive techniques, such as ultrasonic tests, acoustic tests, and rebound hammer tests. To effectively monitor a large-scale civil engineering structure, a large number of discrete transducers must be deployed on the structure, which could be time consuming and cost ineffective in applications. The collected data may require extensive engineering interpretations to provide useful information for engineering designs. Nondestructive techniques are effective tools for the evaluation of a predetermined damage area, which may not be feasible if not impossible in practical applications. Furthermore, they can be used only for a physically accessible portion of the structure. Structural damage may be contributed by load combinations, material flaws and structural deteriorations due to environmental factors. In general, it can occur at any location of a structure. Therefore, it is desirable to develop a system of sensors that are distributed cover the strategically critical locations of the structure.

Distributed sensing systems can be developed with the use of fiber optic sensors and coaxial cable sensors. A fiber Bragg gratings array and a Brillouin scattering time domain reflectometry have been employed to provide a set of distributed data, contrary to localized data by discrete transducers, and an overall picture of an existing structure. They have been proven to be light in weight and of relatively high accuracy (Bao et al., 2001). They can be deployed over a long distance without significant loss in signal strength. They are particularly suitable for tensile strain measurements but less effective for shear strains. The spatial resolution of Brillouin scattering time domain reflectometry

fiber optic sensors is in the order of one meter. The potential drawback with fiber optic sensors is their fragile nature, which requires special cares in harsh construction environment of civil engineering structures.

As a less expensive and more rugged alternative to the fiber optic sensing techniques, coaxial cables were used for crack detection and strain measurement based on the change in their cross section geometry (Lin et al., 1998). Recently a new generation of topology-based crack sensors was proposed and developed by Dr. Chen's research group at Missouri University of Science and Technology or Missouri S&T (Chen et al., 2003). They have been successfully applied into concrete structures using the electrical time domain reflectometry (ETDR) measurement principle for crack detection in concrete members. In this case, coaxial cables are used for both transmitting and sensing devices. When embedded or attached to an RC member, a coaxial cable is subjected to the cracks that develop along the RC member and its ETDR measurements provide information about the severity and location of cracks. The materials used to manufacture ETDR sensors are very rugged; the sensors are an ideal choice for civil engineering applications.

New achievements in a material science brought an era of lighter and thinner materials that increasingly affected structural designs and rehabilitations in civil engineering. For example, fiber reinforced polymer (FRP) sheets have been widely used to externally strengthen the concrete members of existing buildings and bridges. In such an application, the safety of structures strongly depends upon the integrity of FRP sheets. In this case, the size of embedded sensors becomes critical in order to monitor the structural condition of FRP sheets.

1.2. OBJECTIVES

The topology-based crack sensors developed at Missouri S&T have repeatedly demonstrated satisfactory performance in crack detection from the beginning (Mu, 2003) to more recent developments (Sun et al., 2009). Crack sensors were near surface embedded into small- and large-scale RC members, and successfully detected the onset of cracks and monitored their propagation under a gradually increasing load conditions in real time.

This thesis further advances the development of ETDR crack sensors with coaxial cables in three ways: (1) improving the manufacturing process for more uniform sensors, (2) miniaturizing coaxial cables as ETDR sensors, and (3) investigating the effect of sensor attachment methods and media. The previous manual fabrication process of coaxial cables with spiral outer conductors is time consuming; it cannot guarantee the uniform performance of the crack sensors under the same loading condition. The presence of a pre-existing separation between two turns of adjacent spirals on the outer shield of a coaxial cable can affect the sensitivity and spatial resolution of the ETDR sensor. For crack detection in thin composite layers such as FRP sheets, the size of previous ETDR sensors must be reduced. Furthermore, the relative merits of surface attachment and near surface embedment of coaxial cables in applications with the uses of different bonding materials require further investigations.

To address the above issues with crack detection and extend the application of ETDR sensors to corrosion detection, the main objectives set forth in this study include:

1. To develop an automatic, die-cutting manufacturing process for ETDR sensors with coaxial cables,

2. To design and fabricate a miniaturized, distributed crack sensor with validation tests,

3. To investigate the advantages and disadvantages of two installation procedures (embedment versus surface attachment) using various bonding materials, and

4. To explore the feasibility of using coaxial cables as distributed sensors for corrosion detection in steel reinforcement of RC structures.

2. ETDR APPLICATIONS AS A REMOTE QUALITY ASSESSMENT TOOL

The ETDR remote sensing technique has been successfully implemented in various fields. In the early 1950s, it was widely utilized in the field of telecommunication to locate discontinuities along a transmission line (Cerri et al., 2005). Since then, it has been successfully used as a remote electromagnetic sensing technique for damage detection. The ability to convert external disturbances of a transmission line into an electrical output signal makes this technique attractive in structural health monitoring. In general, the ETDR sensing methodology is based on the analysis of the reflected signal from an applied voltage pulse sent through the sensing line at any appreciable discontinuity points. A typical ETDR sensor/sensing line is a coaxial cable that can be characterized by its impedance. The spatial resolution of such a sensor is defined by the electrical properties of the dielectric layer between the inner and outer conductors of the coaxial cable sensor and the rise time of the incident signal.

In the late 1980s, the ETDR methodology was suggested as a tool for soil water content and salinity measurements (Dalton and Genuchten, 1986). Later, Grozic et al. (2000) applied the Time Domain Reflectometry for volumetric water content of soils in loose gassy soils under static and cyclic loadings. In their research, Grozic et al. showed that the signal propagation velocity through the soil is indicative of the dielectric constant which in turn can be related to the volumetric soil water content.

The ETDR methodology has been applied for monitoring the stability of various engineered and natural facilities. O'Connor and Murphy (1997) investigated the stability of crown pillars over abandoned mines. Yin et al. (2009) grouted coaxial cables into

zones that are prone to subsidence and landslide for a real time risk assessment of ground motions. Douding et al. (1987) quantified the type and magnitude of rock mass movement with the ETDR methodology. In their study, coaxial cables were grouted into rock and subjected to tension and shear loading. It was shown that the reflection coefficient from the ETDR measurements is linearly proportional to the applied load.

By using the same concept, Khoshbakht and Lin (2006) demonstrated that the ETDR distributed moisture sensor was capable of measuring the variation of the moisture content in a concrete block.

The idea to use coaxial cables as distributed strain sensors in civil engineering applications was proposed by Lin et al. (1998, 2003). They developed and experimentally validated a mechanical model to relate the loading effect (not strain effect seen in actual applications) on a coaxial cable to the electrical response of the ETDR cable sensor. Commercially available coaxial cables RG-174 were embedded into small-scale RC beams that were tested under a three-point loading scheme. The coaxial cables have an effective dielectric constant of 2.18 and, as strain sensors, have the maximum spatial resolution of 0.16 in (4.064 mm). It was observed that the ETDR signal can be used to pinpoint the deformation pattern of the tested beams and indicate the location of visible cracks. However, the details of the strain measurements were obscured due to the low signal-to-noise ratio of the sensor. In an attempt to improve the sensitivity of RG-174 commercial cables, Lin et al. suggested to substitute the commonly used dielectric material (polyethylene or Teflon) with rubber to facilitate the geometric change of the sensor's cross section.

The geometry-based design of cable sensors for strain measurements may be limited to certain sensitivity since the actual strain applied on the cable in engineering applications is small. Therefore, Dr. Chen's research group initiated a new design of cable sensors with topology changes (Mu, 2002; McDaniel, 2004; Brower, 2007). These efforts have improved the performance of cable sensors for crack detection. Various parameters affecting the design and fabrication of coaxial cable sensors have been investigated systematically.

The newly designed sensors have demonstrated greater potential to reflect the internal condition of a structural member of interest (Chen et al., 2004). In comparison with the sensor studied by Lin et al. (1998, 2003), the topology-based sensor has greater sensitivity (~ 50 times larger) (Chen et al., 2004). The topology-based distributed crack sensors can be used in real time to collect the crack data and information on RC members under dynamic loads such as earthquakes and blasts.

3. GENERAL CONCEPT OF TOPOLOGY BASED SENSORS

3.1. OVERVIEW OF TRANSMISSION LINE THEORY

Any structure designed to transfer energy between two points in space can be classified as a transmission line. This thesis concerns the transmission line formed between the inner and outer conductors of a coaxial cable that can guide an electromagnetic signal. The inner conductor is typically an interior wire while the outer conductor is a cylindrical shield. The space between the inner and the outer conductors is occupied by either air or a dielectric. The shield serves as a return path of a signal on the interior wire; it also assures no communication with the ambient media (Clayton, 1992).

A transmission line can be viewed as a two port network with each port in turn consisting of two terminals as shown in Figure 3.1. The port on the left side of the schematic is a sending end and is typically connected to any circuit such as computer terminal operating in the transmission mode generating an output (generator) voltage. The other port, the right one, Figure 3.1 serves as a receiving end, and is usually connected to a load circuit or simply load, which can be a computer terminal operating in the receiving mode, as illustrated in Figure 3.1.

The energy propagation through the transmission line is facilitated by means of electromagnetic waves propagated inside the coaxial cable. When a voltage source is provided between two conductors at the sending end of the transmission line, electrical current starts to flow within the inner surface of the shielding material and the outer surface of the inner conductor. That generates the electrical field in a radial direction between the inner and the outer conductors and the magnetic field represented by closed circular lines encompassing the inner conductor. The transmission line can be represented

by a continuous electrical circuit with two series elements per unit length - inductance (L) and resistance (R), and two shunt elements per unit length - capacitance (C) and conductance (G), which is defined over a unit length (δx) as illustrated in Figure 3.2.

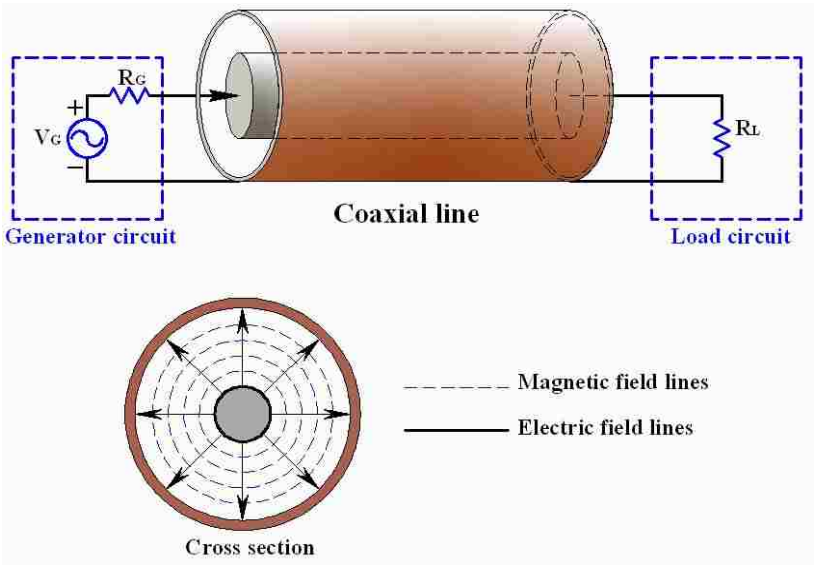

Figure 3.1. Coaxial transmission line

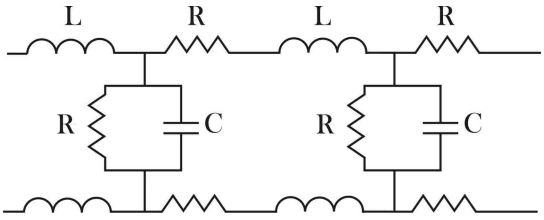

Figure 3.2. Equivalent circuit model

The per unit length resistance accounts for the electrical property of metallic conductors, measured in Ohms/m. It depends upon the conductors' shape and the

frequency operation range. The inductance per unit length is defined by the magnetic field present along the transmission line measured in Henrys/m, which is characterized by the physical parameters of the line, such as shape and separation between the conductors. The transverse electrical field contributes to the per unit length capacitance, measured in Farads/m, and per unit length conductance, measured in Siemens/m. Hence the magnitude of per unit length capacitance depends on the properties of the dielectric material used and its thickness. The per unit length conductance accounts for the leakage of the charge between two conductors and, like the other electrical parameters of a transmission line, depends on the shape and materials used.

One of the main parameters used to characterize a transmission line is its characteristic impedance Z. In any transmission line with a uniform coaxial cable, constant cross section and same material over its entire length, the characteristic impedance is a constant. Hence any discontinuity along a transmission line creates a local impedance change. In other words, when a voltage step pulse is sent through the transmission line, a fraction of the energy reflected back to the sending end at the discontinuity point. The reflected voltage depends upon the magnitude and the character of the discontinuity and can be quantified by a value known as reflection coefficient (Γ):

$$\Gamma = \frac{V^-}{V^+} = \frac{Z_+ - Z_-}{Z_+ + Z_-} \tag{3.1}$$

in which V^-/V^+ represents a complex ratio of the electric field strength of the reflected wave to that of the incident wave, and Z_+ and Z_- are the characteristic impedances of the sensor/coaxial cable before and after the discontinuity, respectively. The ETDR data is

acquired in a time domain at the voltage source end of a transmission line. The magnitude of the reflected voltage is recorded at a delayed time that represents the time elapsed between two points: the incident pulse launch and the reflected pulse arrival back to the recording device. Thus it is straightforward to determine the location of any discontinuity that generates the reflected wave. By using two way travel time, the distance between the two points can be calculated by:

$$x = \frac{vt}{2} \tag{3.2}$$

in which t represents the time required for the signal propagation forward to and back from the discontinuity, and v is the propagation velocity of the signal along the sensing line, which depends on the dielectric constant (ε) and permeability (μ),

$$v = \frac{1}{\sqrt{\varepsilon\mu}} = \frac{c}{\sqrt{\varepsilon_r \mu_r}} \tag{3.3}$$

where the subscript *"r"* indicates relative parameters. Typically the permeability is taken as unity and the dielectric constant of Teflon, often used as a dielectric material for coaxial cables, is approximately 2.1.

3.2. TOPOLOGY BASED SENSOR

Topology-based crack sensor developed at Missouri S&T is based on the mechanism of creating discontinuities at the connection areas of a spiral outer conductor

(Chen et al., 2004). It is a truly-distributed sensing device with high sensitivity and spatial resolution. It mainly differs from the previous designs by Lin (1998, 2003) in the constitution of the outer conductor of a coaxial cable. The previous designs were based on the change in cross-sectional geometry caused by externally applied loading, whereas the new designs by Chen et al. (2004) allow change in the current flow pattern as a result of the change in outer conductor topology.

The new sensor is composed of concentrically arranged metallic inner and outer conductors and a dielectric between them. As shown in Figure 3.3, the outer conductor is formed by wrapping a metal sheet spiral around a dielectric layer. As an example, a prototype cable sensor of approximately 0.15 in. (4 mm) in diameter was used in Chen et al. (2004). The main requirement to the outer and inner conductor is that they must be manufactured with materials of high conductivity so that the current flow along the coaxial cable is not interrupted when connected to a measurement instrument. In this research, tin plated stainless steel (AMS–5606) and tin plated beryllium copper (ASTM–B-194) were used. Tin plated products (spirals) were selected for their superior conductivity and shielding properties.

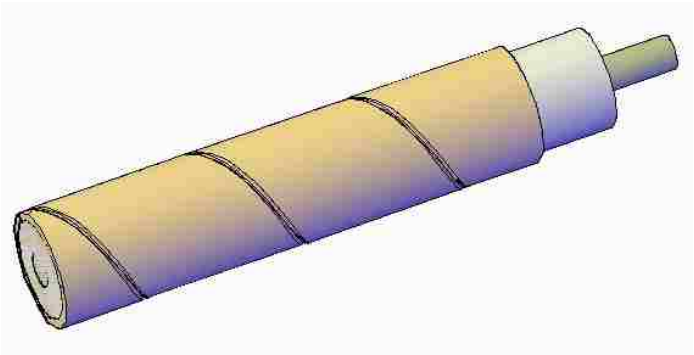

Figure 3.3 Topology-based crack sensor

The dielectric layer can be made from solid polytetrafluoroethylene (PTFE). The fluorocarbon structure of PTFE is a durable, inert material ideal for civil engineering applications. Completely insoluble in most known solvents below 300°C, it has excellent thermal stability and unsurpassed electrical properties, including low dielectric loss, low dielectric constant and high dielectric strength. The rugged constituent components of a coaxial cable sensor make it attractive for structural health monitoring since it can survive harsh manufacturing and construction environments. The service life of cable sensors may be comparable to the design life span of civil engineering structures.

The combination of materials and geometries allows the propagation of electromagnetic waves over relatively long distance in a coaxial cable sensor. The coaxial configuration of the sensor creates immunity to the electromagnetic interference with an ambient environment. As long as the outer conductor can be electrically viewed as a continuous cylinder, the sensor can be considered as a perfect transmission line.

The spirally wrapped outer conductor was used in the topology-based coaxial cable sensors to replace the cylindrical outer conductor of commercial coaxial cables for enhanced sensors' sensitivity to any small mechanical impact (Mu, 2003). To ensure electrical connectivity between the spiral edges and prevent them from separation before loading, a thin layer of copper coating or solder was applied on top of the outer conductor of a cable sensor to enhance the signal uniformity (Brower, 2007). In this way, when the sensor is subjected to either tension or flexure, the local separation between the spiral edges occurs, locally changing the characteristic impedance of the transmission line.

As discussed previously, one of the main factors affecting the propagation mode is the characteristic impedance (Z_0) of a transmission line. For a shield coaxial cable that

does not undergo any changes in its geometry and configuration, the characteristic impedance remains constant over the entire length of the transmission line. In this case, the characteristic impedance can be expressed as a function of distributed elements

$$Z_0 = \sqrt{\frac{R + j\omega L}{G + j\omega C}} (\Omega) \tag{3.4}$$

where the four elements R, G, L, and C are defined before as illustrated in Figure 3.2. When the spirally-wrapped outer conductor of a topology-based sensor remains intact, it can be electrically viewed as a continuous hollow cylinder that shields the internal electromagnetic field from interference by ambient fields, which can be represented by Figure 3.1. At frequencies above 100 kHz, the effects of resistance (R) and conductance (G) become negligible and the transmission line becomes lossless as illustrated in Figure 3.4. The magnitude of the characteristic impedance (Z_o) is then affected mainly by inductance (L) and capacitance (C). In this case, Eq. (3.4) reduces to Eq. (3.5):

$$Z_0 = \sqrt{\frac{L}{C}} (\Omega) \tag{3.5}$$

The inductance and capacitance of a coaxial cable are functions of the inner and outer conductor diameters, and the width of the spirals used for the outer conductor.

Therefore, any change in the configuration of a coaxial cable will affect the characteristic impedance.

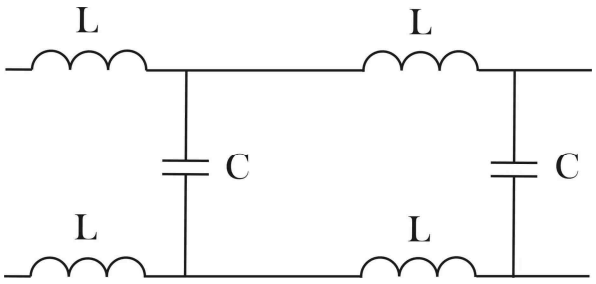

Figure 3.4. Equivalent circuit of a lossless coaxial cable

For example, as a cable sensor is subjected to an increasing external force, the spiral edges of its outer conductor start to separate, resulting in locally disturbed current lines as illustrated in Figure 3.5. The effect of spiral edge separation can be represented by an additional inductance, referred to as a lumped gap inductance (L_{gap}) shown in Figure 3.6.

According to the transmission line theory of a lossless cable, energy sent to the line will travel away the source till it encounters the points of impedance change. At each location, a portion of energy will be bounced back to the source. The strength of the bounced-back signal depends on the effect of the gap inductance and can be characterized by the reflection coefficient that encrypts the information on the separation between spirals of the cable outer conductor. The distributed impedance which is influenced by the gap inductance in a transmission line is one of the key factors to improvement of the distributed crack sensor performance.

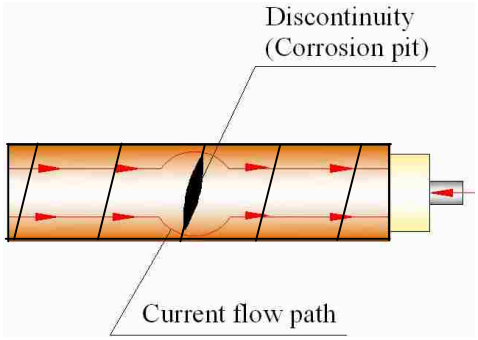

Figure 3.5 Current detour created by discontinuity on the outer conductor

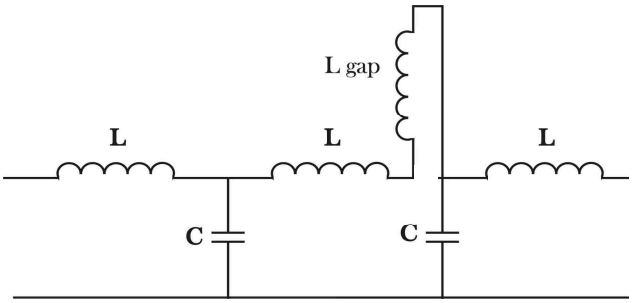

Figure 3.6. L-C equivalent circuit with a lumped gap inductance element

According to Mu (2003) and Wang (2008), the gap inductance is affected by three parameters: the projection of separation length on the cross section plane of a cable, the turn density and the radius of the cable's outer conductor. The sensitivity of a topology-based sensor is a function of its characteristic impedance. The lower the impedance, the more easily the gap inductance can be detected (Mu, 2003). A crack sensor with a high density of spiral turns is expected to provide more accurate information about crack locations since it increases the probability that a crack will coincide with the spiral edges. In this study, one of the improvements made to the crack sensor was thus to significantly reduce the width of the outer conductor spirals.

3.3. DATA AQUISITION

For data acquisitions, either Time Domain Reflectometer (TDR) or Vector Network Analyzer (VNA) can be used for static measurements. The time domain acquisition is desirable since it is easy to relate any event happened in time to a certain special location, as indicated in Eq. (3.2). Compared to VNA, TDR is a more intuitive piece of equipment but has several disadvantages in applications. Its dynamic range is

almost twice lower, resulting in a noisier output signal. TDR launches a step pulse with a fast rising time (~35 ps) signal into the distributed crack sensor, and records the waveform (reflected voltage) bounced back to it by any discontinuity along the cable's/sensor's length, as schematically shown in Figure 3.7. Each discontinuity along the sensor creates a change in impedance which in turn results in a portion of voltage reflected back to the sampling head. The TDR sends a wide frequency range pulse into the sensing line and waits for the response. The reflected signal also contains a wide frequency range, which arrives at the TDR rapidly.

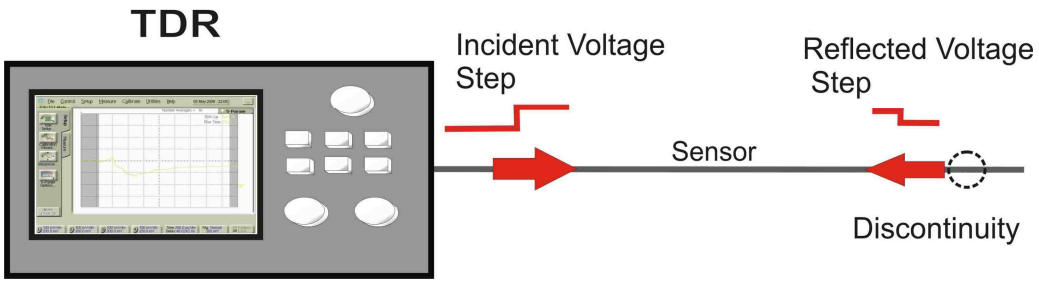

Figure 3.7. TDR working principle

On the other hand, the network VNA sends into the transmission line a single-frequency signal each time within a pre-determined frequency range (100 KHz – 8.5 GHz in this study). The VNA has a built-in band pass filter that is applied to the reflected signal that can reduce the noise level. This process slows down the data acquisition, and is thus more applicable for static measurements.

The measurements with a VNA and relevant settings are explained as follows. The VNA measures S parameters in frequency domain, which are later converted into a time domain. For example, S11 quantifies the ratio of the reflected RF energy to the incident RF energy. Once the data was taken in frequency domain, its inverse Fourier Transform is performed by the VNA with commercial software. With appropriate built-in windowing and filtering in the VNA, a single phase of reflections from a high rise step input is obtained. In this study, data was acquired from miniature crack sensors with the commercial Agilent E5071C 8.5GHz Network Analyzer.

3.4. WAVE BOUNCE DIAGRAM

As indicated in Figure 3.7, a TDR receives the resultant of the incident and reflected voltages over time, which in turn can be converted to a special location along the sensing line where a fraction of the incident voltage was reflected back to the measurement unit. To understand the waveform produced by the TDR, the bounce diagram is discussed here. The bounce diagram is a two dimensional representation of the transient waves bouncing back and forth along a transmission line as shown in Figure 3.8.

Each impedance discontinuity along a sensing line is characterized by a reflected coefficient that defines how much of the transient voltage is bounced back. Figure 3.8 represents a transmission line with a *i* number of discontinuities and the signal traveling back to the monitoring point has to pass through all of them. At each point of the impedance change the portion of the voltage signal, is separated into the reflected wave and the wave that passes through the discontinuity. Thus the apparent, so called reflected

voltage seen at the receiver's screen is the algebraic summation of the effects caused by the reflection at *i*th discontinuity and its subsequent transition through all the previously located discontinuities.

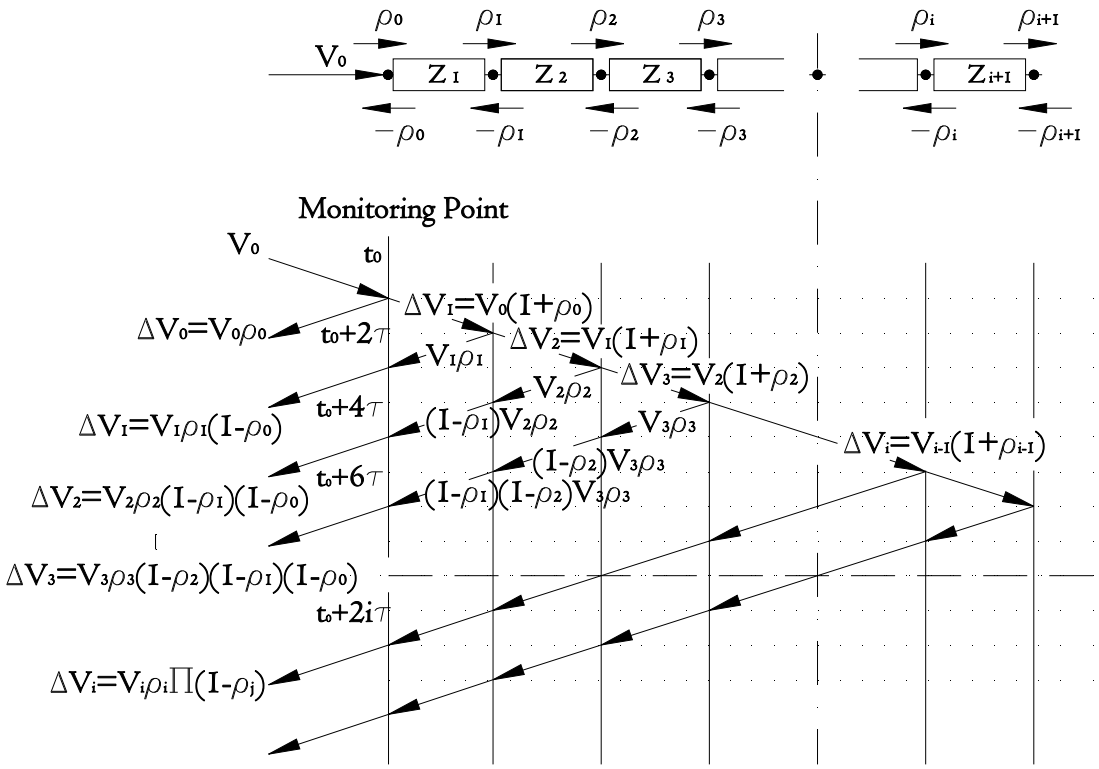

Figure 3.8 Bounce diagram

Thus, by having a voltage wave form as an output, it is possible to back calculate the reflection coefficient and the impedance of the sensing line at each discontinuity. As seen in Figure 3.8, the apparent voltage sampled at the monitoring point is the algebraic summation of the effects caused by each discontinuity that the returning wave passes by. Thus, the true reflection coefficient can be found from the following equation:

$$\rho_i = \frac{\Delta V_i}{V_i \Pi_{j=0}^{i-1}(1-\rho_j)} \quad for \ \geq 1 \tag{3.6}$$

where $V_i = (1+\rho_{i-1})V_{i-1}$ is the voltage of the propagating signal before the *i*th discontinuity, and ΔV_i is the apparent reflected voltage measured by the TDR or VNA. After the true reflection coefficient is known, it is possible to obtain the characteristic impedance distributed profile from the following expression:

$$Z_i = Z_{i-1}\frac{(1+\rho_j)}{(1-\rho_j)} \tag{3.7}$$

It is noted that Eq. (3.6) for ρ_i accounts only for the effect of the primary reflections. It is quite obvious that the signal reflected back to the recording unit will be reflected again and again from all the discontinuities located on its way. This will continue indefinitely. Nevertheless the magnitudes of all the secondary reflections are exponentially smaller than the reflections of the first order and their effect of the apparent voltage is negligible.

4. MINIATURIZED SENSORS FOR CRACK DETECTION

4.1. SPIRALLY WRAPPED OUTER CONDUCTOR

In an attempt to enable the application of topology-based coaxial cable sensors in composite structures with layer configurations, the size of the sensors must be reduced. In this study, a target diameter of 0.067 in. (1.7 mm) of the miniature prototype sensor as shown in Figure 4.1 was considered, which is slightly less than half the diameter of the previous prototype of 1.5 in. (4 mm) in diameter (Mu, 2003). Similar to the previous prototype, a miniature coaxial cable sensor can be fabricated with spirally wrapped outer conductor spirals. The distance between two adjacent spirals, referred to pitch in this thesis, is also half that of the previous prototype as summarized in Table 4.1.

Figure 4.1. Miniaturized crack sensor

The miniature cable sensors were made with the following materials: Inner Conductor - solid silver plated copper clad steel, Outer Conductor - tin plated stainless

steel and beryllium copper, and Dielectric – PTFE. To simplify the manufacture process, commercially available flexible microwave HFE-100D cables were used. The jacket and the outer shielding of each cable were stripped away and substituted by the tin-plated stainless steel (beryllium copper) gasket. This material was selected for its superior spring memory, conductivity and shielding properties. Stainless steel also exhibits excellent corrosion resistance when exposed to humid or salt-fog environments.

Table 4.1. Dimension comparison of two versions of crack sensors

Prototype Sensor	Diameter (in.)		Pitch (in)
	Inner Conductor	Outer Conductor	
Previous Version (Mu 2003)	0.02	0.15	0.14
Miniaturized Version (this study)	0.02	0.067	0.07

As pointed out above, the outer conductor is helically wrapped around Teflon. Due to the smooth nature of Teflon/dielectric's surface, steel spirals can easily slide along the Teflon to ensure that spiral edges are in close contact. Once in place, the steel spirals were painted over with slippage copper-based high conductivity coating (Brower et al., 2008). Each miniaturized crack sensor was terminated with a 50 Ohm impedance load to prevent a significant reflection from the sensor's end.

4.2. DIE CUT OUTER CONDUCTOR

To improve the spatial resolution of sensors so that spiral edges are separated at exactly the same locations as cracks in applications, the pitch of the outer conductor of the sensors must be as small as practically can be. Any impedance discontinuities within

the sensors not associated with the cracks must be avoided. Equally important, to further enhance the uniformity of hand-made prototype cable sensors with spirally wrapped outer conductors coated with either manual or robotic soldering (Brower et al., 2008), a more automatic manufacture process needs to be developed. Any manufacturing flaws or spiral opening present in a coaxial cable causes the attenuation of a propagating signal due to the fringe effect of electromagnetic fields at each opening. Although less of a problem for a short distance, these flaws reduce the measurement distance with the sensors in applications. Soldering with coating does not guarantee a flawless cable due to difficult operations. Furthermore, with spirally wrapped outer conductors, relatively flexible cable sensors are susceptible to bending during handling and installation. For an exploratory study of corrosion detection, unwanted opening of outer conductor spirals may allow inward solution ingress that affects the test results. Therefore, it is imperative to develop a new manufacturing process for cable sensors and overcome the preceding disadvantages associated with the existing crack sensors.

After several trials, a die-cut automatic manufacturing process is developed in this study. To facilitate the new process, UT-09C-35 semirigid coaxial cables with a characteristic impedance of 35 Ohm (www.microcoax.com) were selected. Their outer conductor is made of a continuous thin walled copper cylinder. The diameter and thickness of their outer conductors are 0.09 in. (2.29 mm) and 0.008 in. (0.2 m), respectively. The die-cut prototype sensor is shown in Figure 4.2.

The die was selected to cut the thread in such a way that the only about three forth of the outer conductor thickness is affected by the die cutting. In this way, the cable sensor remains shielded over its entire length and the current flow is not interrupted

unless it is loaded. At the same time, the grooves on its outer conductor make the cable much more susceptible to cracking under external loads.

Figure 4.2. Die-cut crack sensor

Since it is relatively rigid, the sensor remains its original shape during installation and uncontrolled bending is minimized. In addition, the die-cut sensor has a finely ribbed surface, promoting a better bond between the sensor and the host material in applications and eliminating their potential relative slippage or ambiguity in data interpretation. The baseline ETDR measurements of a spirally-wrapped and a die- cut crack sensor are compared in Figure 4.3 and Figure 4.4. As one can see, the waveform from the die-cut sensor has fewer aberrations caused by fabrication defects than that of the sensor with the spirally-wrapped outer conductor around its dielectric.

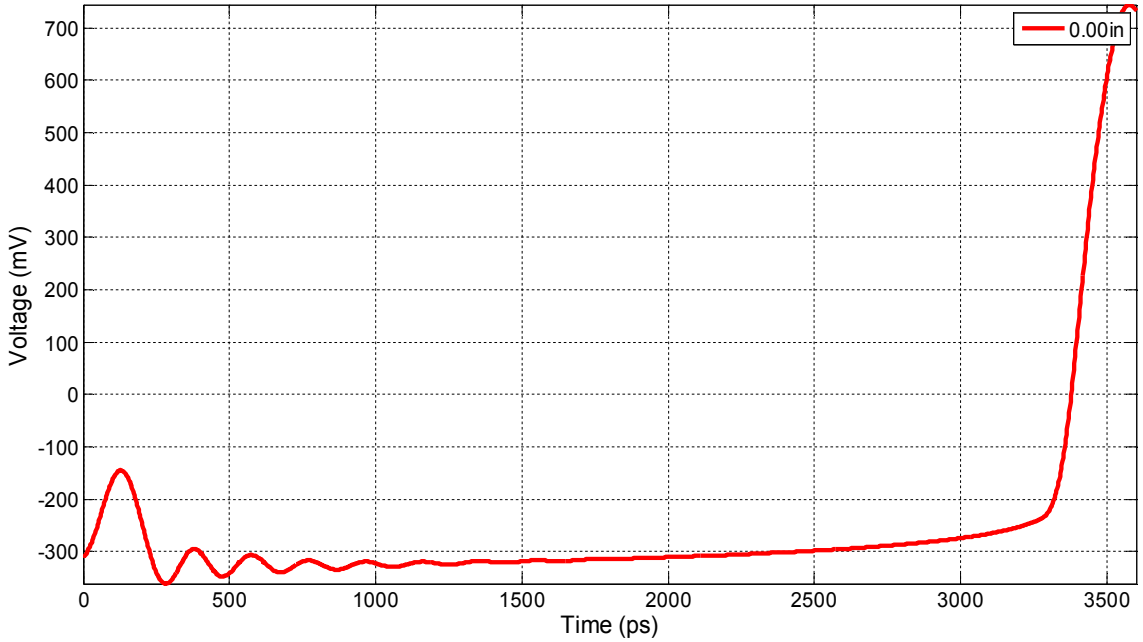

Figure 4.3. Baseline reading from the die-cut crack sensor

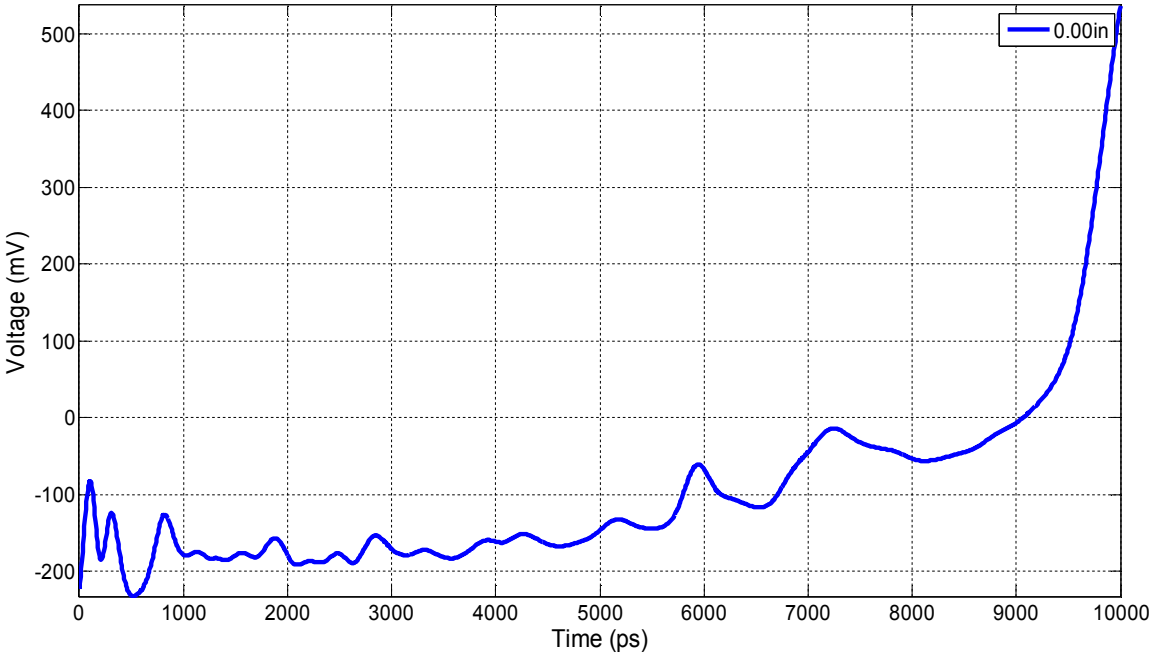

Figure 4.4. Baseline reading from the crack sensor with spirally-wrapped tin plated copper outer conductor

4.3. INSTALLATION PROCESS

To evaluate the performance of miniaturized crack sensors, small-scale RC beams were tested under three point loading. For comparison, both miniaturized crack sensors and their previous prototypes were fabricated and installed into small-scale RC beams. For practical applications, unless crack sensors were embedded into a RC structure during casting, it is critically important to select right adhesive materials that can sustain various environmental and loading conditions but break as cracks in sensors' host material penetrate through the adhesive materials.

When a crack sensor is rigidly attached to a RC element, the stresses developed in the element are transferred directly to the sensor. Note that the crack sensor can only detect a crack that develops across it. Thus during the installation process, the orientation of expected cracking should be taken into considerations.

All sensors were placed along the tension face of the tested beams. Each beam was instrumented with three (3) topology-based sensors. As shown in Figure 4.5, two sensors were embedded into 0.5 in deep precut grooves and one sensor was attached to the tension face of the beam along its center line. The goal of this study was to select the best way for installation of the above mentioned crack sensor. Two types of installation (embedded vs. surface attached) were compared. For each installation type, various types of adhesive materials are compared, including grouting (SikaGrout212), epoxy (HoldTight®102), structural resin (M_BRACE Saturant), and mortar with a weight mixture of 1 part of Portland cement, 0.5 part of hydrated lime (type S), and 3.5 to 4.5 parts of masonry sands according to ASTM-C-144. The test matrix is given in Table 4.2.

Figure 4.5. Grouting procedure

Table 4.2. Test matrix for installation methods and materials

Beam #	Embedded			Surface Attached		
	SikaGrout212	Mortar I (PC)	Mortar II (PC_Epoxy)	SikaGrout212	HoldTight®102	Structural Resin
2		xx			x	
3	xx				x	
4			xx			x
5		xx				x
6		xx				
7			xx		x	
8		xx		x		
9		xx		x		

4.4. EXPERIMENTAL VALIDATION OF SENSOR PERFORMANCE

Ten 36-inch long beams of 6”×6” cross section were designed for flexural failures with 4.5 ksi normal concrete and Grade 60 steel rebar. Four beam were reinforced with #3 and six beams were reinforced with #4 rebar and all of them had #3 cross ties, as illustrated in Figure 4.6. For comparison, two embedded sensors, one miniaturized and one previous prototype (Type-1) by Mu (2003), were deployed at the symmetric locations as shown in Figure 4.6.

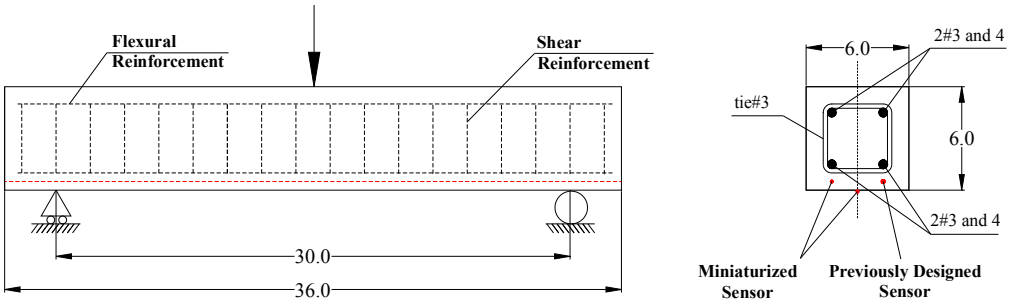

Figure 4.6. Test specimen and three-point flexure test setup

The surface attached sensor was with miniaturized designs. All sensors were fabricated with spirally wrapped outer conductors with copper soldering since the die-cut manufacturing procedure was developed toward the end of this study. Copper coating atop the outer conductor of a cable sensor introduces additional friction between the sensor and RC member, creating strong bond between them.

A 200 kip Tinius Olsen Universal Testing Machine was used for all tests as shown in Figure 4.7. A gradually increasing load was applied at the 0.1 in/min crosshead displacement rate. At each 0.01 in interval at the compression face, a TDR signature was

recorded. A linear variable differential transformer (LVDT) was set up between the crosshead and the specimen platform of the test machine, giving the mid-span deflection of the beam. Data was acquired with an Agilent Technologies E-5071C 100 kHz - 8.5 GHz Network Analyzer that was operated in the Time Domain Reflectometry (TDR) mode.

Figure 4.7. Three-point bending test setup

5. EXPERIMENTAL VALIDATION OF CRACK SENSORS

5.1. MINIATURIZED VERSUS PREVIOUS PROTOTYPE SENSORS

The load-crosshead displacement curve of the Beam #2 is illustrated in Figure 5.1. It can be seen that the slope of the curve changes at 0.15 in crosshead displacement, indicating the upper limit of elastic behavior. Section of the curve bounded by 0.15 in corresponds to the behavior when tensile stresses at the bottom of the beam have gradually reached the tensile strength of the concrete. Most of the cracks have been developed in this region. It should be noted that the kinks on the curve are results of an applied load relaxation due to pauses taken to record TDR signatures from the sensors installed on the tested beam.

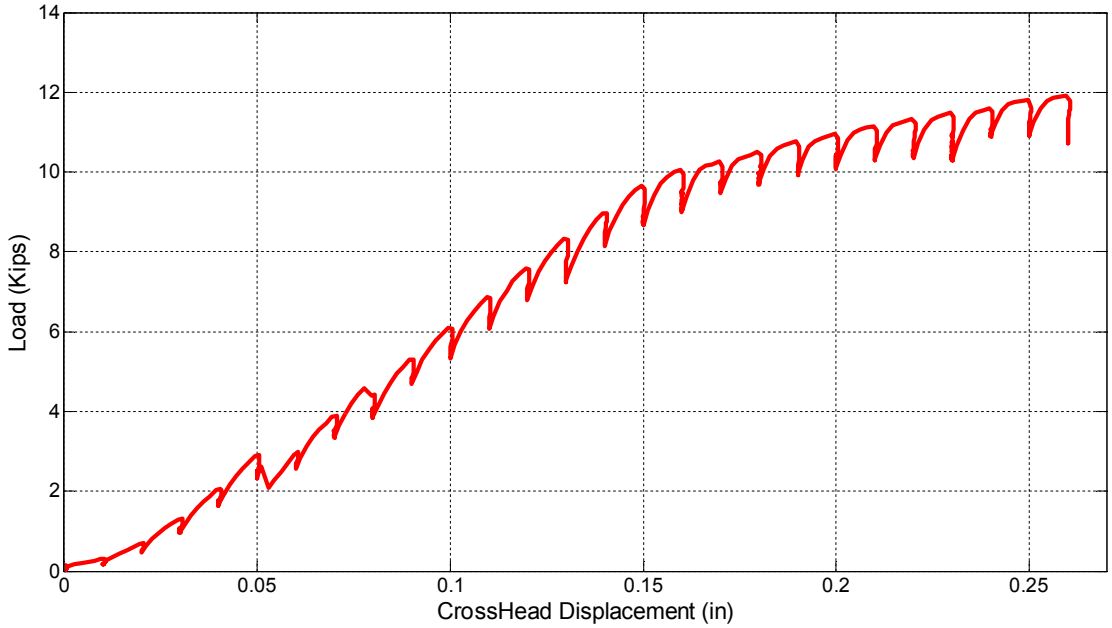

Figure 5.1. Load-displacement curve

Figure 5.2 compares the normalized waveforms acquired from the previously designed (Type-1) by Mu (2003) and the miniaturized sensor; both sensors were embedded into the grooves. Each curve reflects the impedance change caused by sequential 0.01 in (0.254 mm) crosshead displacement increments. The minimum crack that can be detected by naked eyes is approximately 0.0079 in. (0.2 mm) wide. According to the full wave simulations done by Sun et al. (2009), the minimum crack width detectable by the crack sensor is less than 0.1 mm. In the experiment described in Section 4.4, the first noticeable impedance deviation was recorded in the middle portion of the beam at a crosshead displacement of 0.05 in (1.27 mm) while no cracks were observed on the tested beam surface. This phenomenon can be explained by the fact that the sensor can "feel" stresses developed in the surrounding concrete right before first crack develops.

The TDR signature corresponding to a crosshead displacement of 0.06 in (1.53 mm) included a prominent spike at 21.4 ns (19 in) from the left end of the beam. As soon as the first spike appeared, the beam was visually inspected and no apparent crack lines were observed at the surface. It suggests that the sensor was able to pick up a very beginning of the crack opening when its aperture is less than 0.0039 in. (0.1 mm). At the next increment of crosshead displacement, the first crack has been observed. That was followed by an impedance increase on the TDR signature that corresponds well to the physical location of the crack. At the crosshead displacement of 0.14 in (3.56 mm), the second spike was recorded at about 19.5ns (~13 in) from the left end of the sensor. That was immediately followed by the second crack development at 13.75 in from the left support of the beam, Figure 5.2.

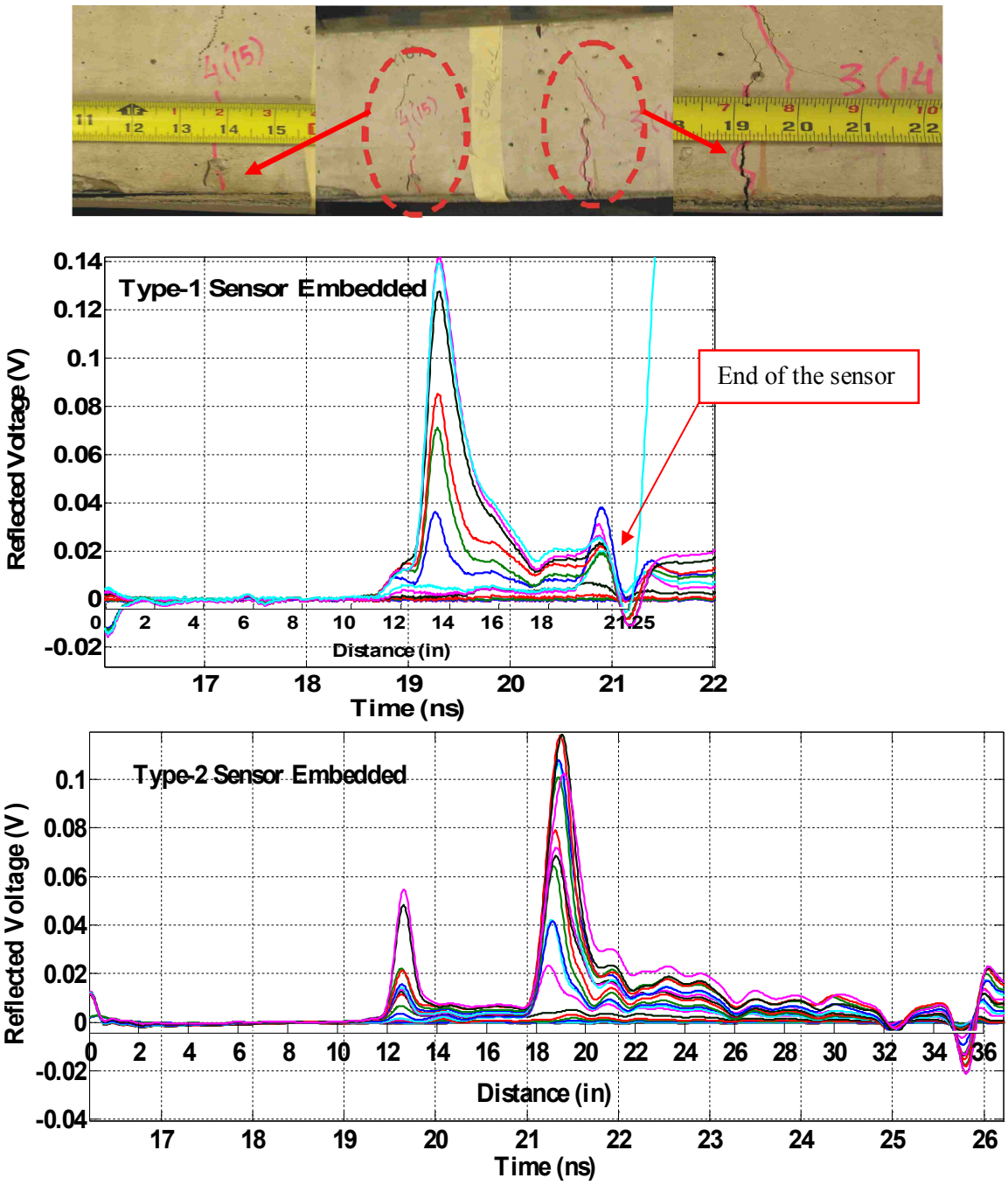

Figure 5.2. Crack pattern and TDR responses from the previously developed sensor (Type-1) and the miniaturized sensor (Type-2)

As the load level continued to increase, the amplitude of the reflected voltage increased gradually. The spike, corresponding to the first appeared crack, progressed

more dramatically than that of the second one due to nonlinear stress redistribution after the first open crack. Since the sensor was embedded into the beam, the stress was directly transferred to the sensor.

The TDR signatures from the previously developed and miniaturized sensors were compared. It is noticed that the pulses on the TDR waveforms recorded from the miniaturized sensor are slightly narrower (less area occupied under the local spike waveform) than those from the previously developed sensor. Therefore, the miniaturized crack sensor tends to provide more accurate information on the location of the cracks developing along the beam or have higher spatial resolution. It is also noted that the reflection coefficient detected by the miniaturized sensor for the crack developed at 13.75 in from the left support is almost twice less than that of the one detected by the previously designed sensor. As mentioned previously, the characteristic impedance of the sensor significantly affects its sensitivity. Due to limitations of the commercial components used in this study, the characteristic impedance of the miniaturized sensor is 50 Ohm, significantly larger than 15 Ohm for the previously designed crack sensor. As such, the sensitivities of the two sensors cannot be compared in a fair way.

The miniaturized sensors are more sensitive to the stress concentration during the first stages of loading when that means that the miniaturized sensor, due to its refined geometry, begins to deform earlier than the previously designed sensor. Figure 5.3 illustrates TDR signatures acquired at the same crosshead displacement from the miniaturized and previously designed sensors placed in one beam. It is obvious that the miniaturized sensor attached to the tension surface of the beam first detects concentration

of stresses at the mid-span region, while the previously designed sensor at that stress level has a high noise-to-signal ratio.

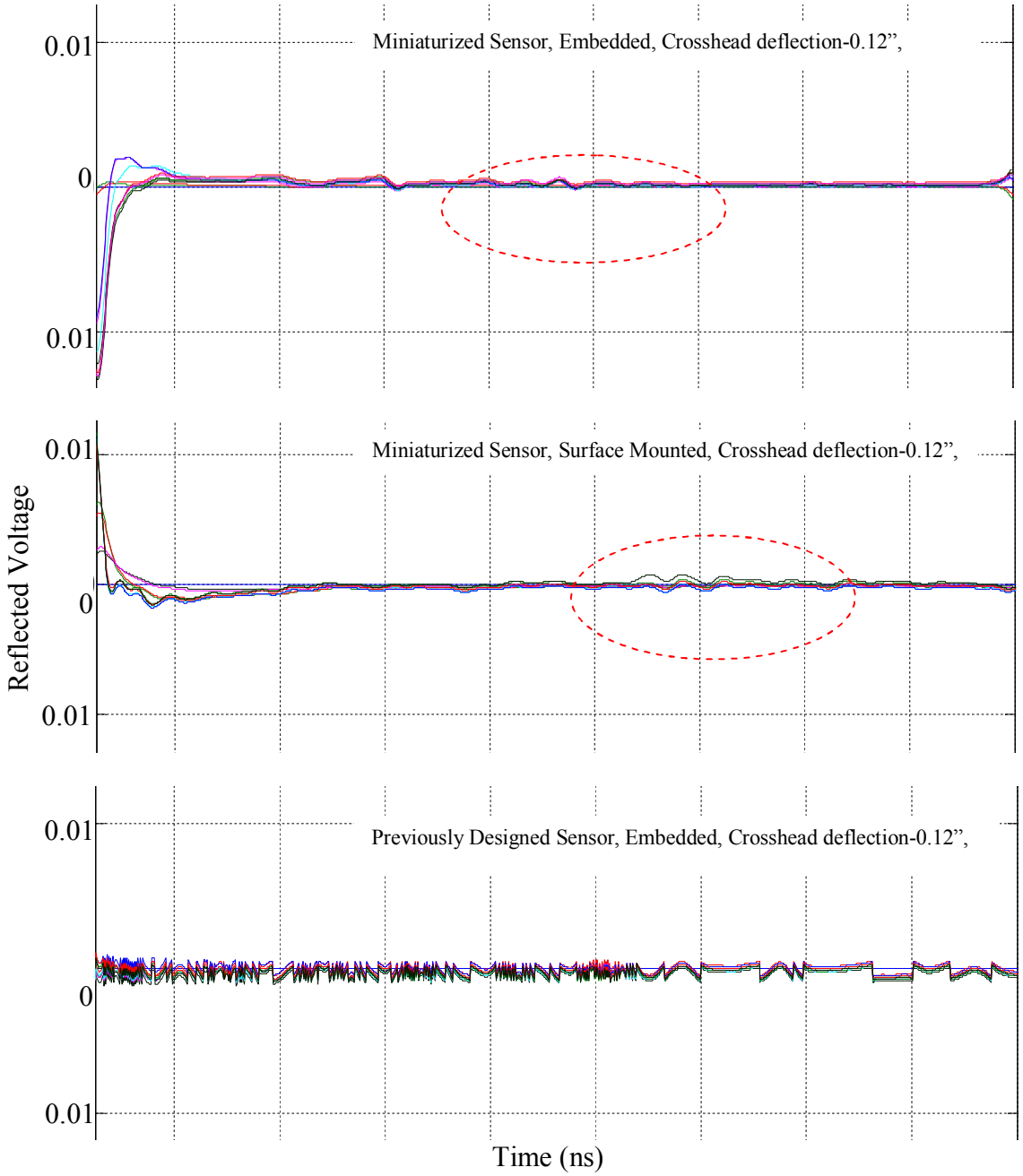

Figure 5.3. Comparison of the waveforms recorded from the previously designed and the miniaturized sensors

5.2. EMBEDDED VERSUS SURFACE ATTACHED MINIATURIZED SENSORS

Figures 5.4 through 5.21 show the TDR data recorded from the miniaturized sensors installed in Beams #2 to #7. In all figures, embedded sensors are marked as sensors #1 and #2, whereas all surface attached sensors are identified as sensor #3.

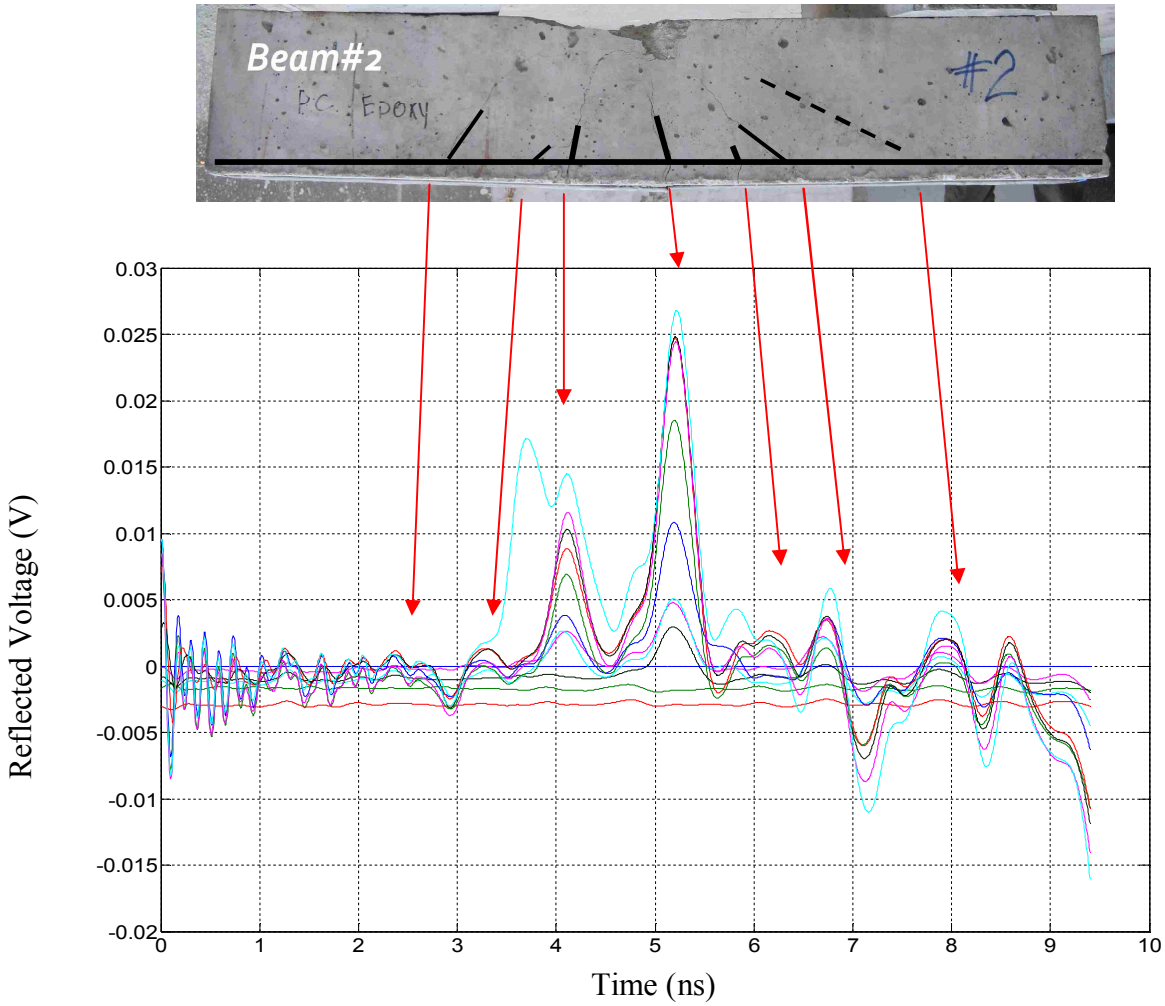

Figure 5.4. Crack pattern of Beam # 2 and TDR signatures from Sensor # 1: embedded with Portland cement

For better bond between the mortar grouting material and the host material, the installation grooves were pretreated with primer. As shown in Figure 5.4 and Figure 5.5, the embedded sensors provided the waveforms that are in general agreement with the crack patterns observed on the tested beam. All visible cracks have been clearly identified by the spikes on the TDR waveforms. The progression of cracks and the widening aperture of the spiral separation are shown by the increasing magnitude of the reflection coefficient and the locally increasing area under the TDR signature. Note that the connection for Sensor #1 was slightly loose during the test, resulting in a signal disturbance up to the first 2.5 ns.

The same adhesive material was used to install the second embedded sensor. As shown in Figure 5.5 all cracks were detected fairly well. The waveform patterns from the first sensor, Figure 5.4, and the second sensor, Figure 5.5, are quite similar, which can be used to cross verify the accuracy of the information yielded by both sensors. The waveforms also indicate additional spikes at about 6 ns and 7.3 ns, suggesting the presence of smaller cracks of width less than 0.0039 in. (0.1 mm) that were not detected during the visual inspection.

On the other hand, the surface attached sensor with HoldTight®102 adhesives behaved differently. As shown in Figure 5.6, the crack pattern within the adhesives is different from that of the RC beam. The surface attached sensor appeared to respond to the cracks in the beam and the adhesives, giving the TDR waveforms that quite differ from the crack pattern on the beam. Thus the surface attachment with HoldTight®102 is ineffective to transfer the cracks from the beam to the sensor.

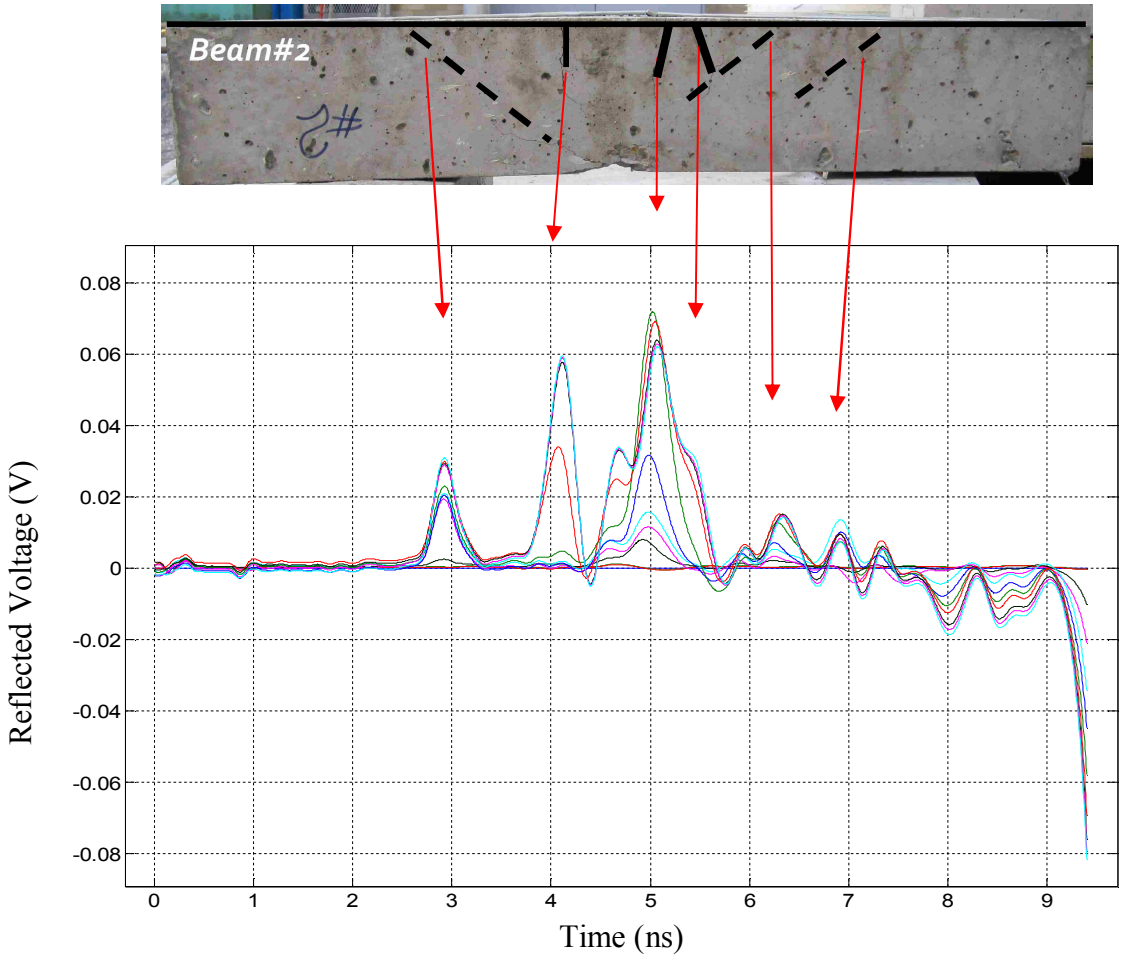

Figure 5.5. Crack pattern of Beam # 2 and TDR signatures from Sensor # 2: embedded with Portland cement

Figure 5.8 and Figure 5.9 illustrate the crack patterns and the TDR waveforms acquired from Beam #3 with two embedded crack sensors that were installed with SikaGrout 212 adhesives. As indicated in Figure 5.8, the correlation between the crack pattern within the beam and Sensor #1 response is considered to be satisfactory. All significant cracks were detected correspondingly.

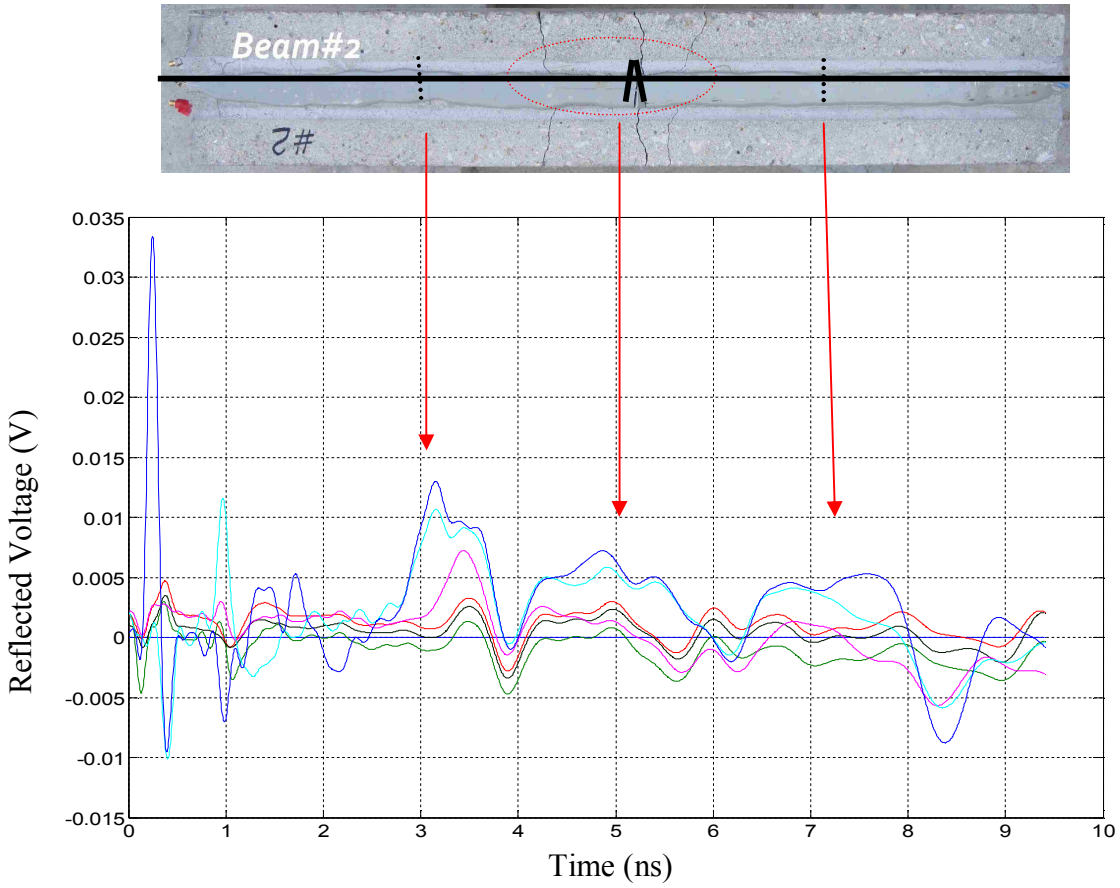

Figure 5.6. Crack pattern of Beam # 2 and TDR signatures from Sensor # 3: surface attached with HoldTight

In addition, the surface attached sensor is also susceptible to spalling as evidenced at midspan of the beam in Figure 5.7.

Sometimes along a beam peripheral, cracks terminate before reaching the layers of the sensor installation. For Beam #3, such situations occurred at approximately 8.3 in and 27.7 in from the left support, the zones marked by dotted lines in Figure 5.8. The embedded sensor experienced tension stresses, thus initiating local spiral separations as seen in Figure 5.8 at 3.3 and 8.5 ns.

Figure 5.7 HoldTight 102 spalling at the midspan of Beam # 2

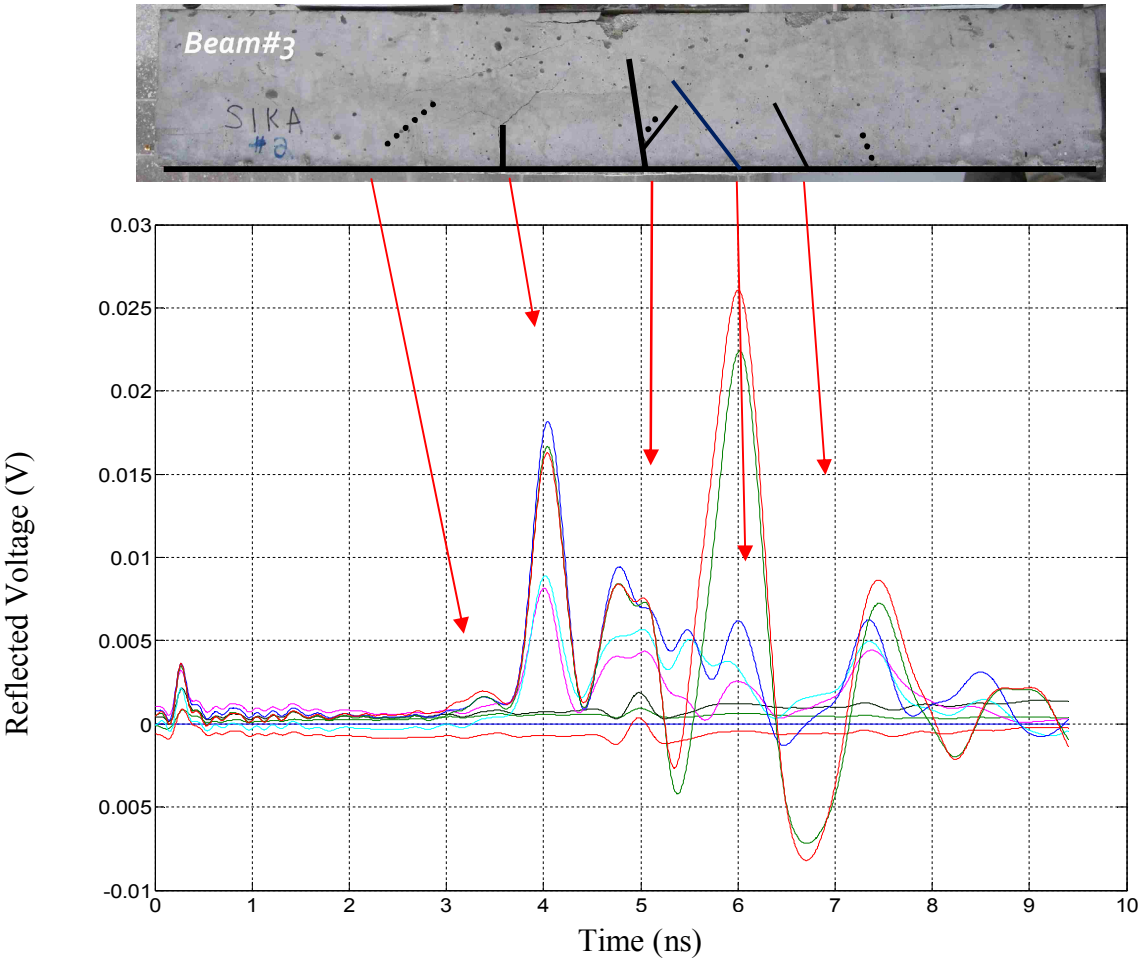

Figure 5.8. Crack pattern of Beam # 3 and TDR signatures from Sensor # 1: embedded with SikaGrout 212

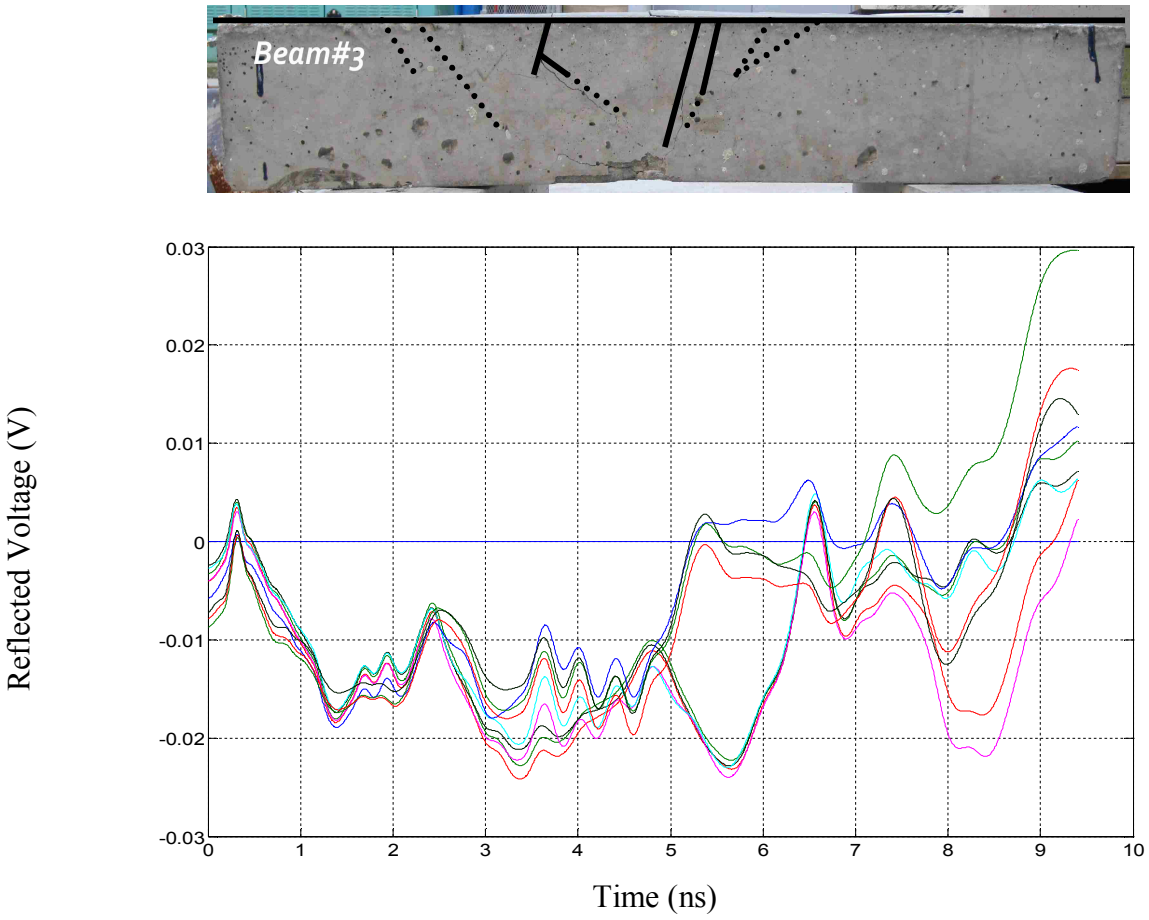

Figure 5.9. Crack pattern of Beam # 3 and TDR signatures from Sensor # 2: embedded with SikaGrout 212

The second embedded sensor was damaged during the installation. As shown in Figure 5.9, the TDR signatures completely missed the crack distribution. For a remote structural health monitoring, it is critical to understand how the crack sensor response should look like. In the case of the normalized data, a sensor attached to the tension face of a structure should have most of the positive reflected signatures above the time/location axis. The damaged sensor can also be identified by incoherent waveforms over time as seen in Figure 5.9.

Sensor #3 was surface attached to Beam #3 with Hold Tight ® 102 adhesives. As shown in Figure 5.10 and Figure 5.11, the adhesives delaminated at midspan. The crack patterns on the beam and the sensor are different. The surface attached sensor tended to respond to the crack patterns from both materials and is thus ineffective.

Figure 5.10. Crack pattern difference between Beam # 3 and Sensor # 3 and delamination of HoldTight 102 adhesives at midspan

The crack patterns developed on the surface of Beam #4 together with the waveforms acquired from the miniaturized crack sensors are illustrated in Figure 5.12 and Figure 5.13. To enhance attraction between grouting and the host materials, the grooves molded on the tension face of the beam were brushed with the primer. The sensors were grouted with the mortar. During the beam transportation, one of the embedded sensors was damaged. As seen in Figure 5.12, location of all cracks within the beam is reflected fairly accurately by the TDR signatures. In addition, the sensor suggests the presence of the crack zones missed by visual inspection.

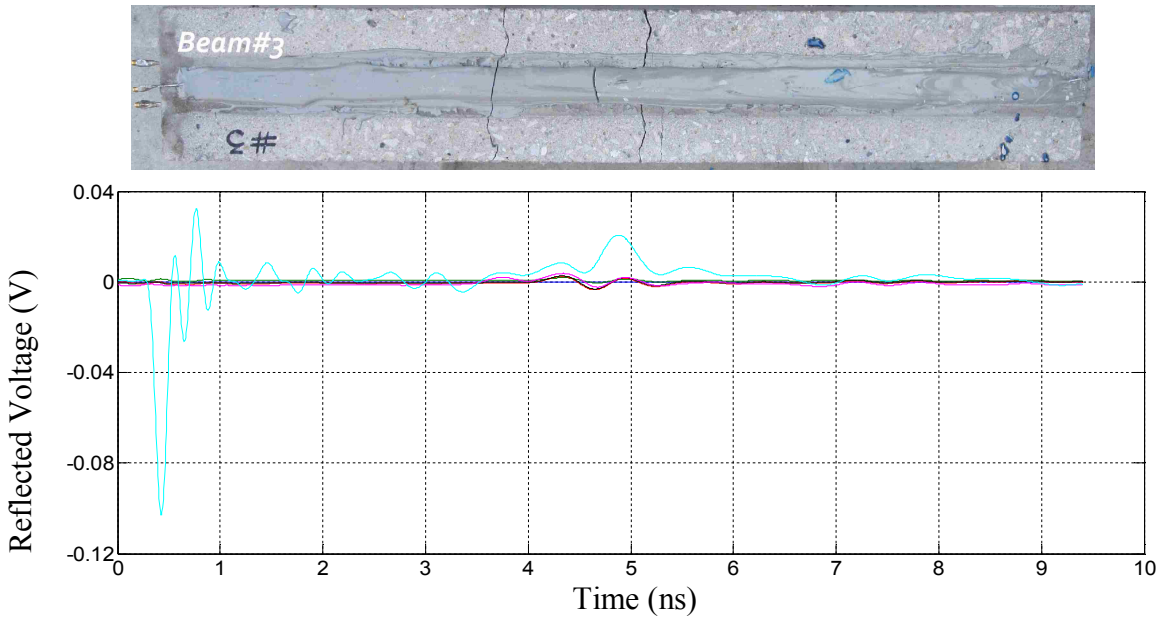

Figure 5.11. Crack pattern of Beam # 3 and TDR signatures from Sensor # 3: surface attached with HoldTight 102 adhesives

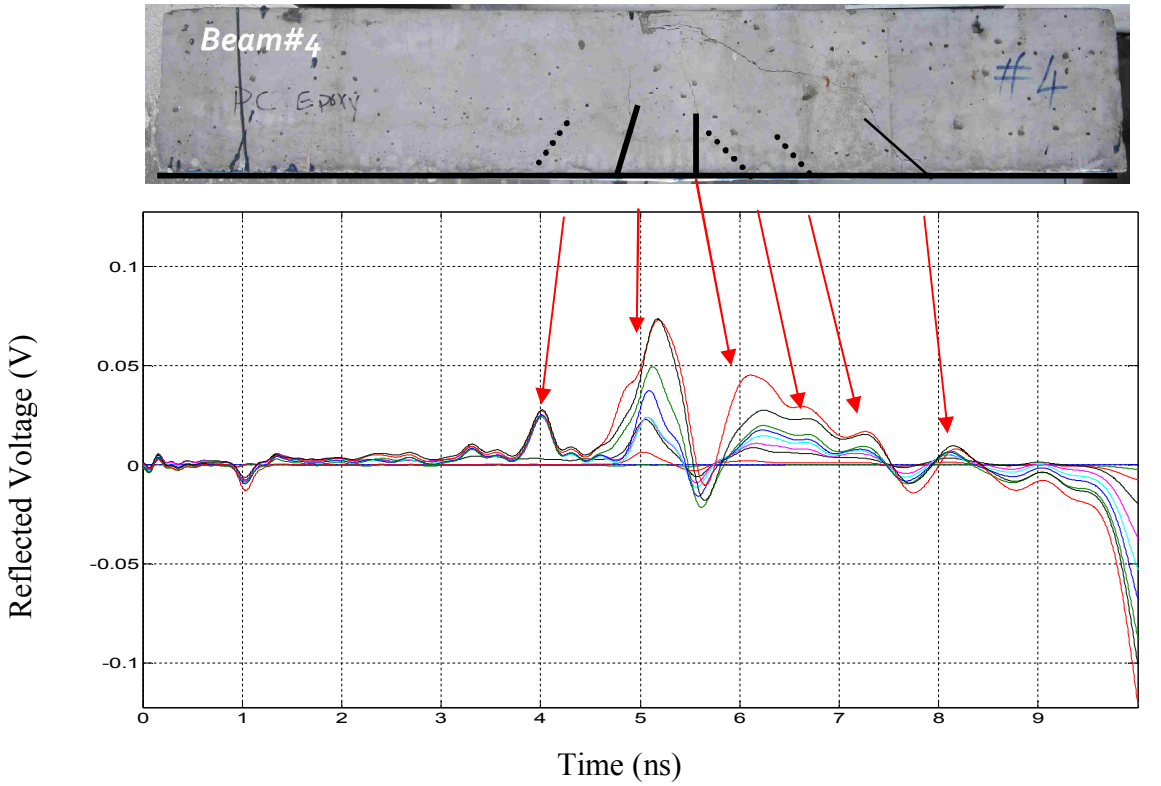

Figure 5.12. Crack pattern of Beam # 4 and TDR signatures from Sensor # 1: embedded with mortar

For the surface attachment on Beam #4, M_BRACE Saturant was used. A thin layer was poured over the sensor as shown in Figure 5.13. The adhesives, similar to HoldTight102, behaved differently than the concrete in tension. It appeared to be more tension resistant and eventually developed fewer but wider cracks than the tension face of the concrete beam. Thus the surface attached sensor was affected by the differential behavior of the concrete and the adhesive which resulted in an erroneous data,

Figure 5.13.

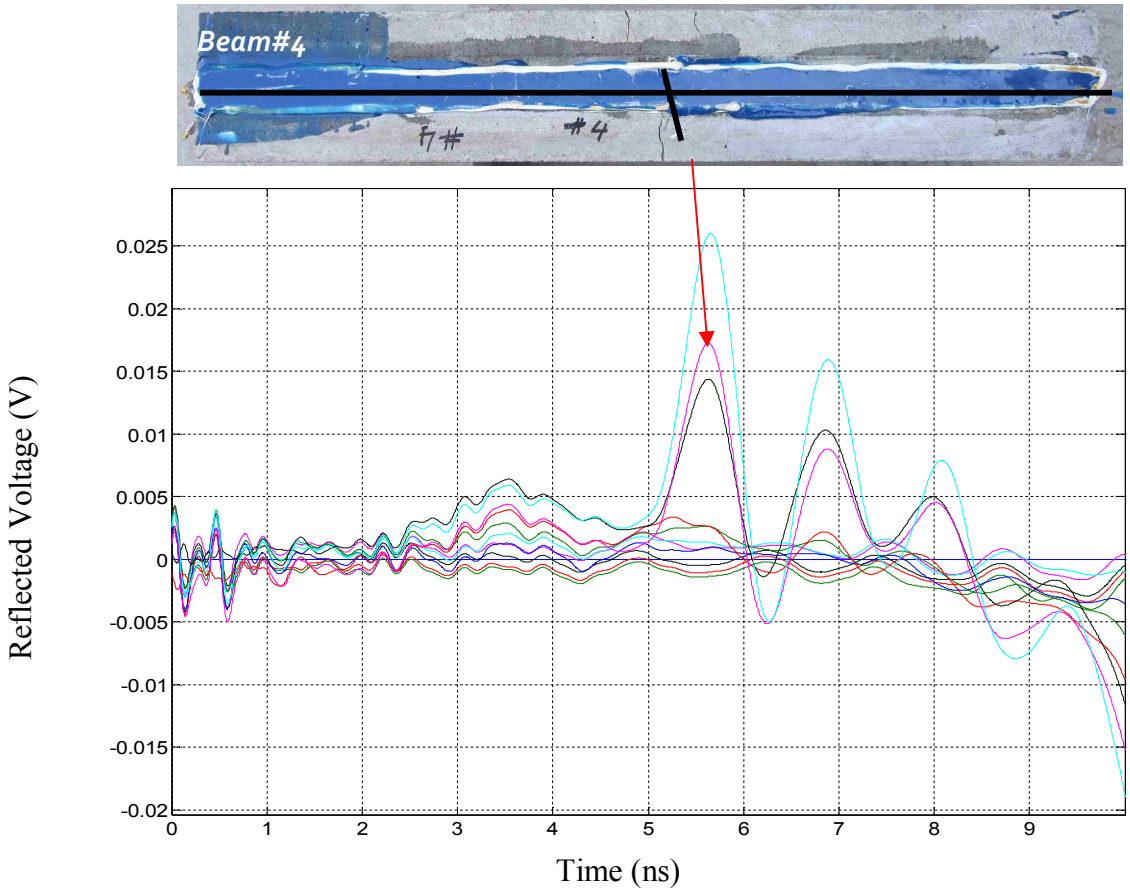

Figure 5.13. Crack pattern of Beam # 4 and TDR signatures from Sensor # 3: surface attached with structural resin (M_BRACE Saturant)

The close-up view of the middle section of the beam is shown in Figure 5.14. In this case, no delamination is observed of the structural epoxy (M_BRACE Saturant). However the fact that the sensor does not respond to the crack pattern within the structural element itself suggests that the adhesive material cannot be used for the crack sensor surface attachment.

Figure 5.14. Crack pattern difference between Beam # 4 and Sensor # 3

For Beam #5, the embedded sensors were installed with mortar and the surface attachment was done using structural epoxy (M_BRACE Saturant). Figure 5.15–Figure 5.17 illustrate the crack patterns and the normalized TDR waveforms acquired sequentially under gradually increasing loading on the beam. As indicated Figure 5.15 and Figure 5.16, Sensors #1 and #2 can detect the cracks on the beam accurately. The connection of the first sensor was loose with an exceptionally large reflection originated there. It resulted in a less energy sent through the sensor. Nevertheless it behaved adequately. The series of the reflections within the first and third nanoseconds Figure 5.15, are caused by the higher stresses within the beam at the corresponding location.

There were cracks observed on the side surface of the beam that had not reached at the tension fibers of the beam where the sensor was grouted. The fact that all visually available cracks were identified correctly, suggests that the additional spikes on the TDR signatures (at 6.5 s and 7 ns) are produced by smaller cracks that were not visually seen on the beam's surface, Figure 5.16.

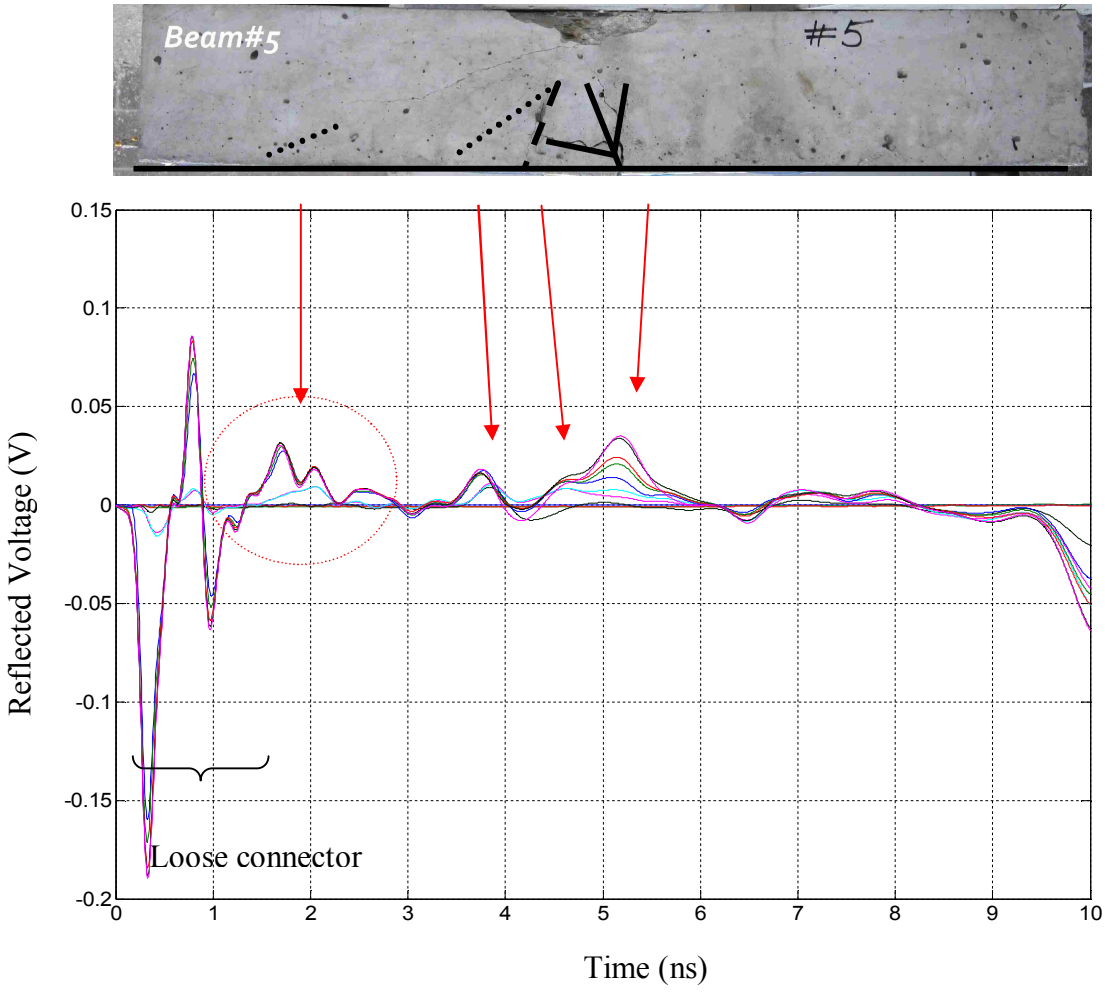

Figure 5.15. Crack pattern of Beam # 5 and TDR signatures from Sensor # 1: embedded with mortar

It can be seen from Figure 5.17 that the surface attached sensor detected three possible cracking zones on the tension face of the beam whereas the structural resin exhibits only one immense discontinuity at the midspan of the beam. This suggests that the adhesive material improves the overall behavior of the beam and is not suitable for the surface attachment of sensors, since it has higher tensile strength than the concrete used in the beam.

For Beam #6, two sensors were embedded with mortar. Figure 5.18 and Figure 5.19 indicate that all visually detected cracks were correctly detected by the sensors.

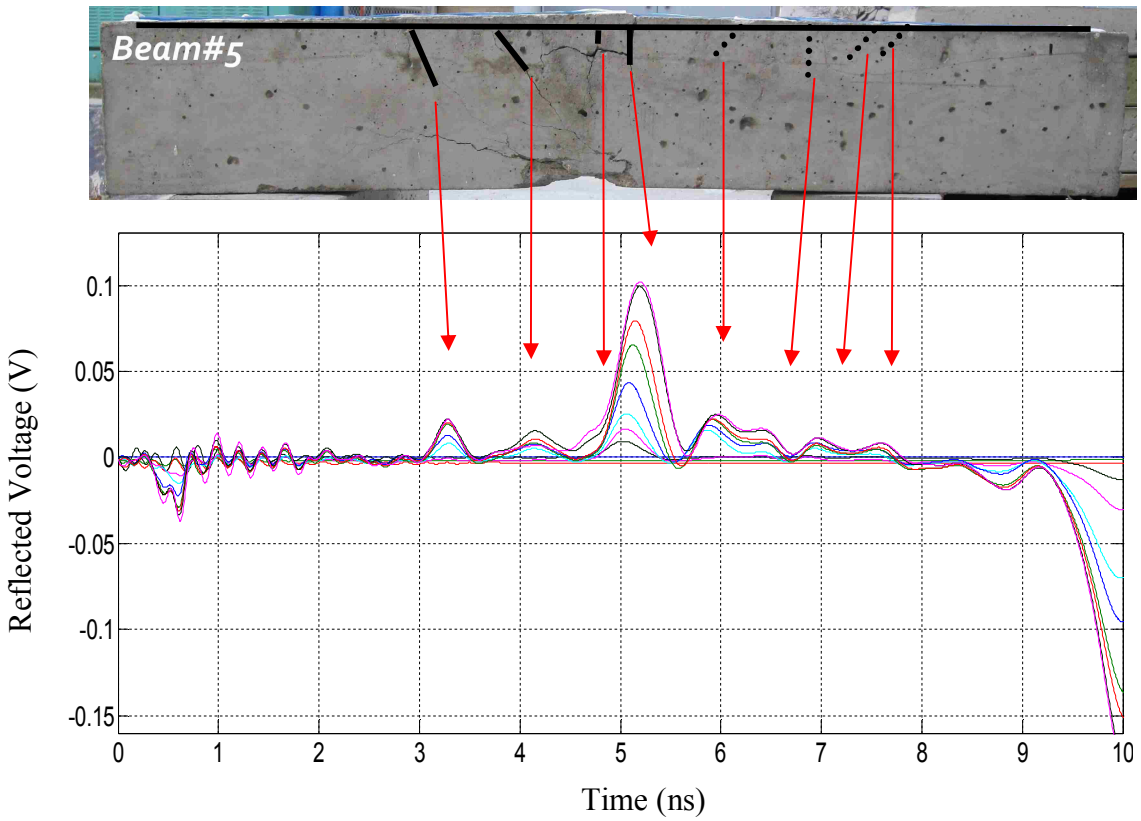

Figure 5.16. Crack pattern of Beam # 5 and TDR signatures from Sensor # 2: embedded with mortar

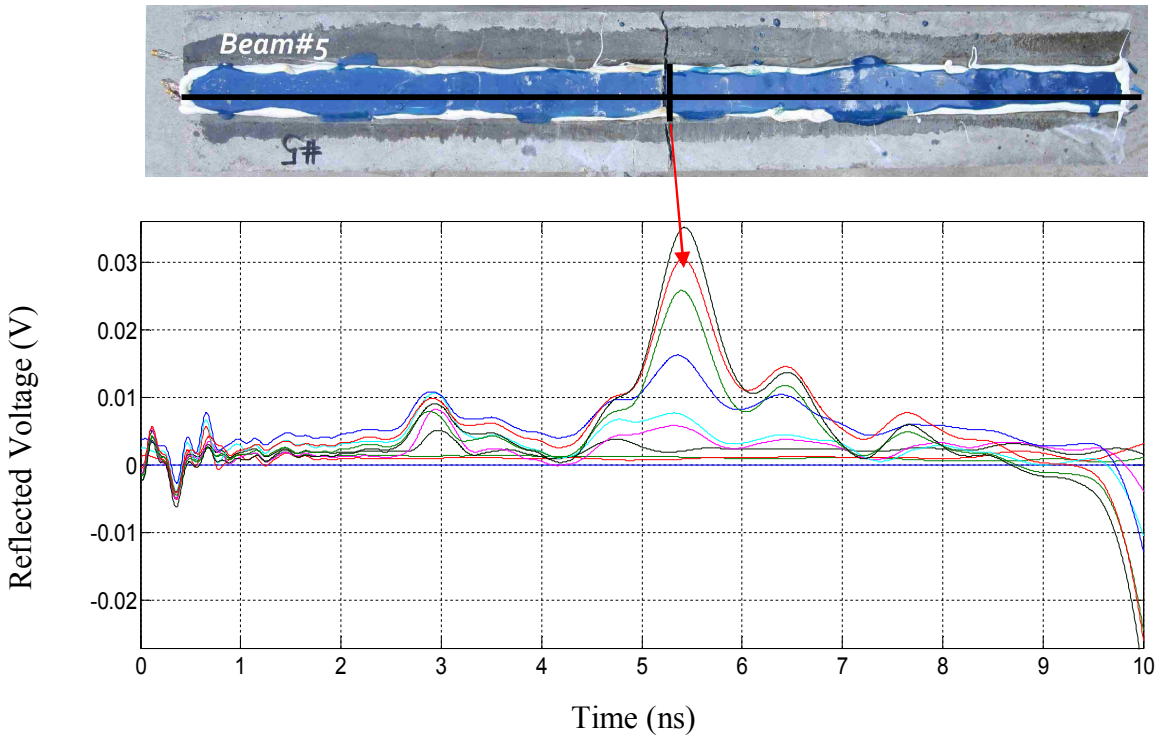

Figure 5.17. Crack pattern of Beam # 5 and TDR signatures from Sensor # 3: surface attached with structural epoxy (M_BRACE Saturant)

The area where the crack had not reached the crack sensor location by the end of the test is marked by the red ellipse. This is where the tensile stresses within the beam compelled the separation of the spiral edges in the outer conductor of the sensor, resulting in additional inductance and hence the series of reflections at this location, Figure 5.18.

As shown in Figure 5.19, the second embedded sensor detected all the cracks except the one marked by the yellow line. The exception was due to the fact that the crack changed direction before it reached to the groove and the sensor as shown in Figure 5.20, the crack continued to grow along the groove but never crossed the sensor

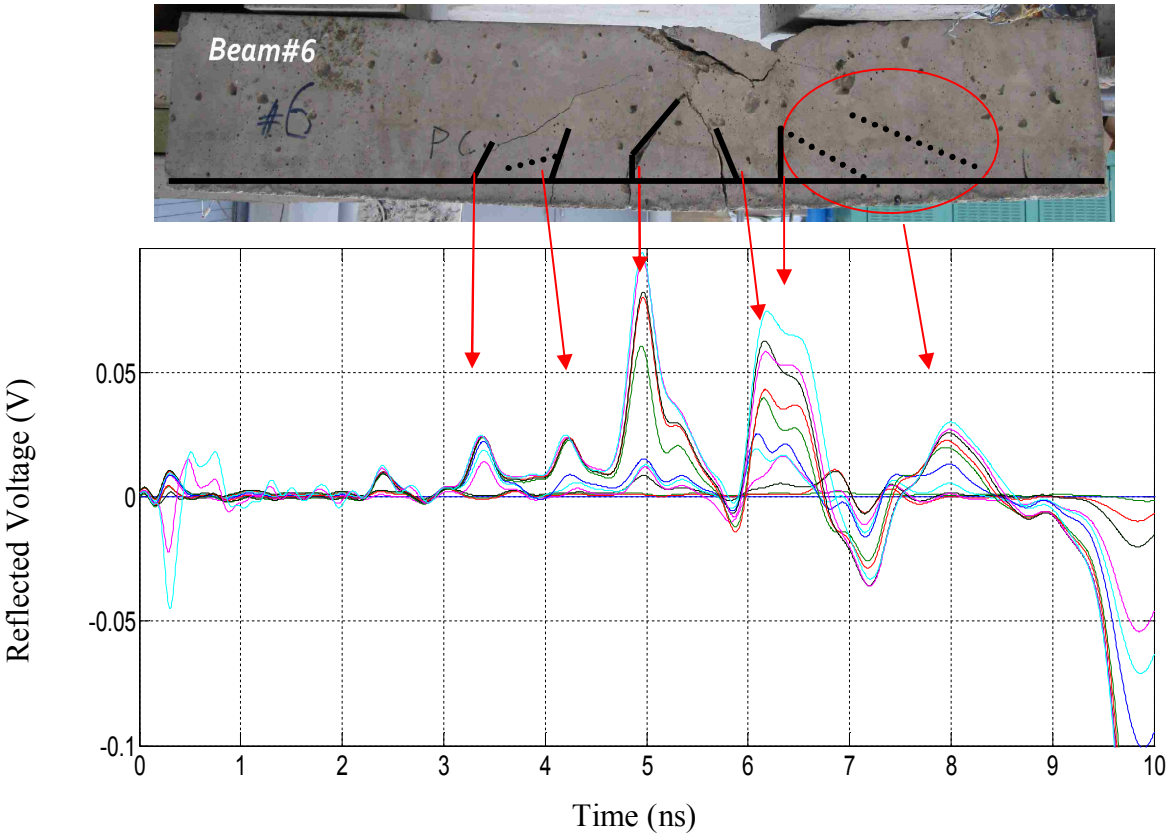

Figure 5.18. Crack pattern of Beam # 6 and TDR signatures from Sensor # 1: embedded with mortar

For Bean #7, one embedded sensor was installed with mortar, and one surface attached sensor was installed with HoldTight®102. Figure 5.21 presents the crack pattern and TDR signatures from the embedded and the surface attached sensors. It can be seen from Figure 5.21 that the embedded sensor successfully detected all visible cracks.

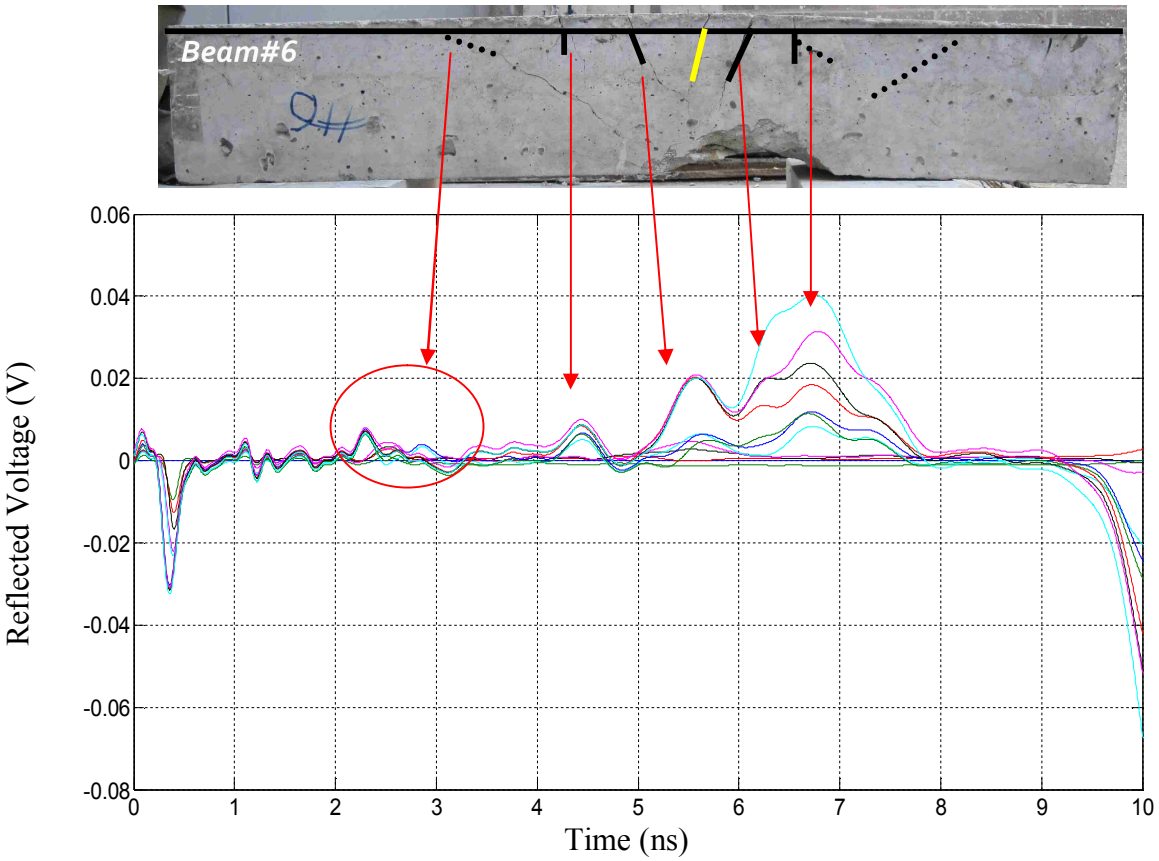

Figure 5.19. Crack pattern of Beam # 6 and TDR signatures from Sensor # 1: embedded with mortar

Figure 5.20. Close-up view of the crack pattern within the midspan of the tension face of the Beam # 6

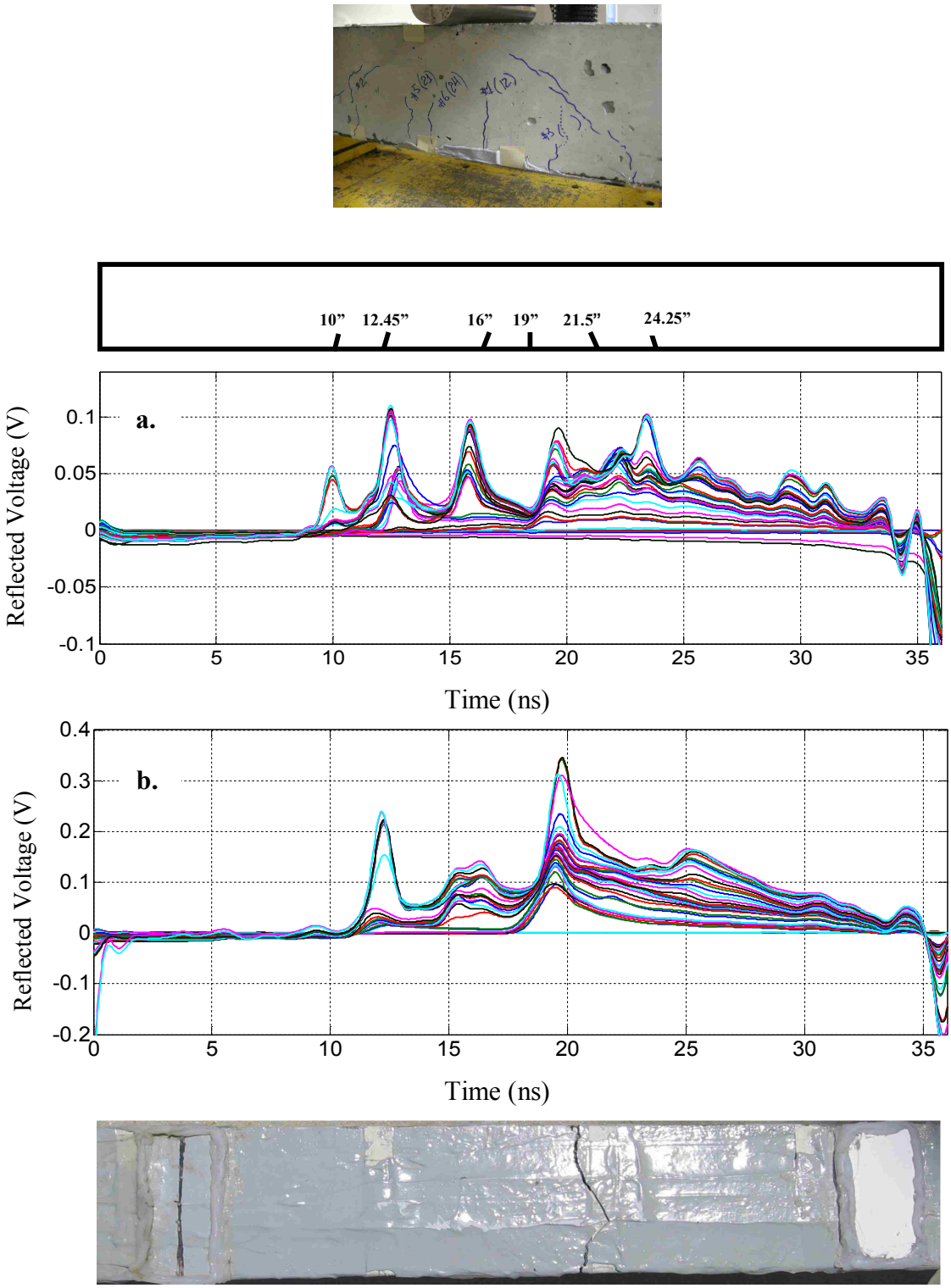

Figure 5.21. Crack pattern of Beam # 7 and TDR signatures from the Beam # 7 from (a) embedded sensor, and (b) surface attached sensor

However, the surface attached sensor mainly detected the crack pattern on the adhesives, which is quite different from that of the beam. Therefore, the surface attachment is not recommended.

5.3. CONCLUSIONS

The comparison between the previously developed crack sensor and the miniaturized sensor has shown that the refined geometry of the miniaturized sensor can improve spatial resolution in crack detection. Due to limitation with commercially available parts, the sensitivity comparison cannot be made on a common basis of equal characteristic impedances. Nevertheless, the waveforms obtained under ambient conditions indicate that the energy reflected by the previously designed sensor is almost twice higher than that of the miniaturized sensor. Despite the higher impedance, the miniaturized sensors thus yielded satisfactory results, successfully detecting all cracks of 0.1 mm or wider. Moreover, they can identify cracks that are invisible to naked eyes during visual inspections. This suggests that the sensitivity of the miniaturized sensor is quite satisfactory. Note that, if deemed necessary, the characteristic impedance of a miniaturized sensor can be lowered by reducing the distance between the inner and the outer conductor.

By comparing TDR signatures acquired from sensors with different installations, it can be concluded that the surface attached sensor detected the upcoming crack earlier than that embedded into a host structure such as RC beams. This general trend is consistent with the structural mechanics theory since the extreme fiber of a beam, where surface attached sensors are located, is subjected to cracking first. However, surface

attached sensors are susceptible to spalling and delamination from the beam. More importantly, in most cases, the surface attached sensor appeared to experience a stress condition combining the effects of crack patterns both in the beam and the adhesive material. Among various installation materials, SikaGrout 212 can ensure a good bond of surface attached sensors with the beam. The sensors attached with SikaGrout 212 appeared more responsive to the cracking patterns than other adhesives such as HoldTight®102 and M_BRACE structural epoxy since they exhibit higher tensile strength than the normal weight concrete and tend to inhibit deformation of the outer conductor of the sensors. This resulted in a delayed response to the crack propagation.

The general criterion for the selection of installation adhesives is to ensure that the selected adhesives have the same or less tensile strength than the structural member of interest. In practical applications, mortar grouting is recommended for sensor embedment and SikaGrout 212 is recommended for the surface attachment of sensors. To enhance the bond between the host and the adhesive materials primer can be introduced.

6. CABLE SENSORS FOR CORROSION DETECTION

6.1. INTRODUCTION

Corrosion processes in steel reinforced structures can result in structural deficiency and with time create a threat to human lives. According to the Strategic Highway Research Program (SHRP) of the U.S. National Research Council, the average annual cost of corrosion by the end of 1989 was about $8.3 billion (Koch, et al., 2001). By the end of 2000, the U.S. annual cost of corrosion was estimated from 325 to 1000 million of EURO per year. This only accounts for the direct cost from the highway bridge infrastructure deficiency due to corrosion. The indirect cost coming from traffic delays and lost productivity can be up to ten times greater. Prompt retrofit and effective maintenance can extend the structures' live span at much less expenses. Corrosion monitoring techniques can provide realistic information on the location and the severity of corrosion that are crucial for the development of an effective structural preservation strategy.

6.2. CORROSION MONITORING AND DETECTION

Corrosion is a naturally occurring process commonly recognized as deterioration of ferrous material when it reacts with the environment. Commercially available techniques for corrosion monitoring and detection are in the form of nondestructive test and evaluation. They are limited to local operations and time consuming to cover a wide area associated with large-scale civil infrastructures.

Among various nondestructive evaluation tools are half-cell potential tests, linear polarization tests, macro-cell current measurements, concrete resistance & resistivity

measurements, and electrochemical impedance spectroscopy tests. Some of these methods require costly equipment and certain interpretation skills. To the best of our knowledge, none of the above techniques is designed for real time quality assessment.

In this study, the crack sensor developed at Missouri S&T is proposed as a distributed sensor for real time corrosion monitoring. Implementation of the proposed technology may ease the pressure on bridge owners restrained with the federal budget by allowing the timely remediation with the minimal financial and labor expense. Cable sensors, as discussed in Section 3, are instrumented such that the location of a discontinuity developed along its length can be easily detected. When a sensor is placed in an immediate vicinity to the steel reinforcement, it is subjected to the same chemical processes as the steel reinforcement. In this case, corrosion pitting is expected to develop on the sensor exactly at the same location as in the rebar. Thus coaxial cable sensors expect to be an effective tool for active corrosion zones detection within RC members.

A series of laboratory tests were conducted to explore the feasibility of using coaxial cables as corrosion monitoring devices. Nine sensors were manufactured and placed in the artificially created corrosive environment and observed over the time. To induce accelerated corrosion, 3% and 5% NaCl solutions were used. Based on the test results, the proposed distributed sensor is capable of delivering fairly accurate information on the location of a discontinuity along the sensor caused by the corrosion pitting. Forensic study was also conducted to confirm some of the observations. In order to test corrosion sensors in application conditions, 27 cable sensors were prepared and placed into RC beams. The beams have been placed in a salty sand bath and are currently under continuing tests. ETDR readings will be taken from the corrosion sensors in the

duration of tests and any signs of corrosion will be monitored over the time. The corrosion test results of the RC beams will be reported in a future document.

6.3. REINFORCED BAR CORROSION

One of the main reasons why many RC structures become structurally inadequate in the U.S. National Bridge Inventory is steel reinforcement corrosion that is followed by concrete degradation caused by the high tensile stress exerted by expanding corrosion products around the steel. Figure 6.1 briefly illustrates the corrosion process of steel rebar in a concrete block due to deicing salt.

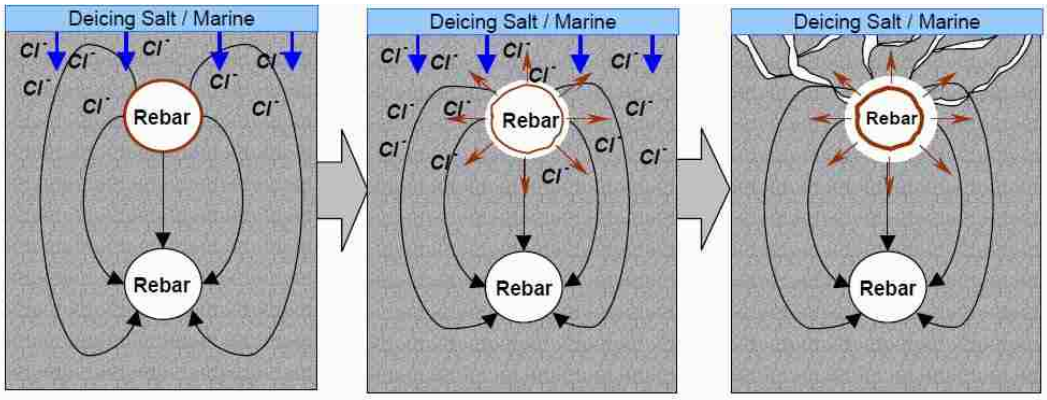

Figure 6.1. Schematics of rebar corrosion in a concrete block

Concrete in its nature is a porous media with a relatively high pH level (~12.5). At the early stage of concrete, all voids within it are filled with an electrolyte primarily made of potassium and sodium hydroxides. When reinforcing steel is subjected to an alkaline environment, its surface typically gets covered with a thick and adherent iron oxide film. This passive film protects reinforcement from further degradation. As the

concrete gets carbonized over time from the atmosphere and infiltrated with deicing salts (mainly NaCl), the alkali in concrete is neutralized and the pH level is lowered, leading to a breakdown of the protective iron oxide coating and the beginning of corrosion.

Corrosion rate is controlled by several factors: availability of moisture, concentration of corrosive agents (salts and access of oxygen) and temperature. The oxidation process forms a residue that does not firmly adhere to the surface of the steel and flakes off easily causing reinforcement expansion. That imposes radial stresses on the surrounding concrete and indirectly instigates formation of micro cracks. The cracking provides more intense ingress of carbon saturated meteoric moisture and corrosion rate progressively accelerates. Extensive oxidation within steel reinforced members eventually weakens RC structures.

6.4. CORROSION SENSOR

The implementation of a distributed crack sensor has been proven to deliver fairly accurate information on the location of a discontinuity, particularly a crack crossing the sensor embedded within a RC member. This happens because the transverse crack creates a foot print on the outer conductor of the sensor.

Since the corrosion process within a reinforced structural member can result in the formation of a corrosion pit along the embedded sensor, it (the sensor) presumably can also be used for location of the zones with active corrosion processes within RC members. As shown by Brower (2007), the vicinity of a metal rod has little or no effect on the quality of data provided by the sensor. Thus, from the point of view of electromagnetic interference, the sensor can be safely placed fairly close to the rebar,

such that both of them are subjected to the same corrosion environment (corrosive agents). As alkalinity of concrete goes down, corrosion pits are expected to appear on the sensor's surface and on the surface of reinforcement. With laboratory calibration, the measured sensor corrosion rate can be related to the corrosion process of steel reinforcement. The sensor used in this study has its outer conductor made of beryllium copper which is susceptible to oxidation processes in a carbonized and chloride concentrated environment. When copper cover undergoes pitting corrosion, the electrical uniformity of the outer conductor is interrupted. As a result impedance of the sensor at the corrosion affected spots starts to increase gradually with the increasing size of the corrosion pit. This phenomenon can be dissolved into the location of a weakened section and degree of rebar deterioration caused by corrosion. To validate the hypothesis that crack sensors can detect corrosion, a proof-of-concept corrosion test was conducted.

6.5. CORROSION TEST DESCRIPTION

The preliminary corrosion tests were conducted in an aqueous environment. The metal exposure to a high humidity environment is known to accelerate the oxidation process. The other factors affecting the rate of corrosion are the presence of salts and temperature. The presence of the dissolved salts improves the conductivity of the aqueous solution and increases the rate of electrochemical corrosion.

Two sets of experiments were conducted. In the first test series, three prototype corrosion sensors were placed into 3% wt NaCl in distilled water solution (Montemor et al., 2000). The sensors were made as described in Section 3 except that the stainless steel outer conductor with the following copper coating was used. In the second test series,

nine sensors were prepared with the beryllium plated copper outer conductor for a faster corrosion reaction in comparison with the first test series. The sensors were placed into distilled water, 3% and 5% NaCl solutions. Different solution compositions were used to better control the corrosion processes. Both experiments were conducted at a constant room temperature (~75°F). For the data acquisition, Time Domain Reflectometer (TDR) (Agilent Infiniium DCA-J 86100C) and Network Analyzer (E5071C, 100 kHz-8.5GHz) were used.

6.5.1. The First Test Series. TDR signatures were collected at the time when the sensors were submerged and every fifth day of a week after beginning of the test. The TDR signatures are presented in Figure 6.2.

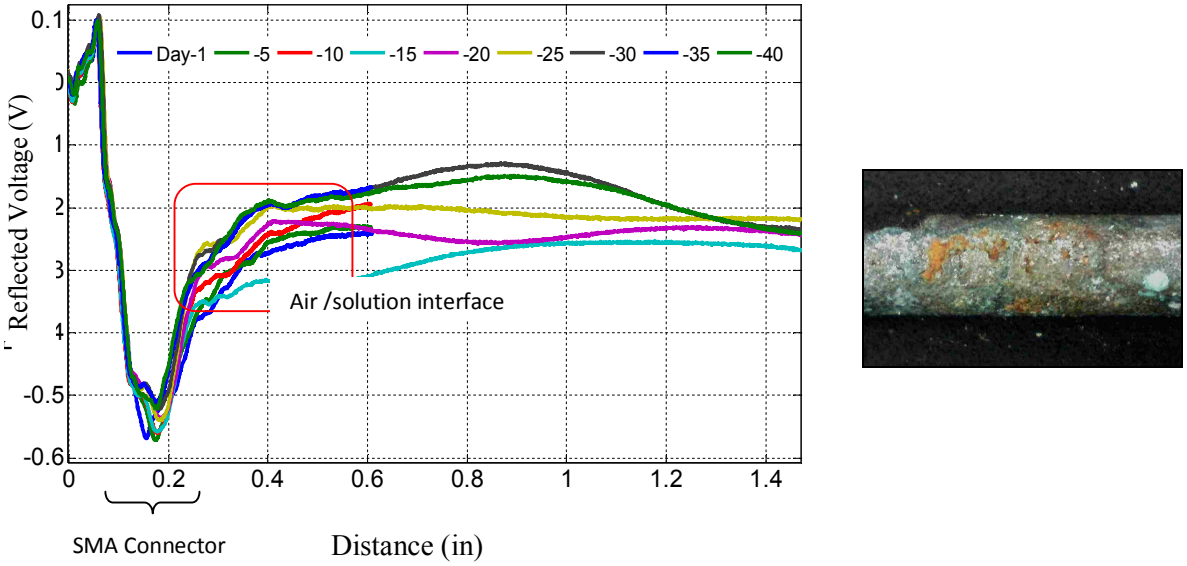

Figure 6.2. TDR signatures taken at every fifth day after beginning of the corrosion test

It can be seen from Figure 6.2 that the overall impedance gradually increases with the passage of time. The results can be explained by the fact that the connectivity at spiral edges of the outer conductor decreases as the thin copper coating layer gradually dissolves in the oxidation process. The TDR signatures clearly indicate the SMA connector region and the air/solution interface where most of the oxidation took place. The photo illustrates the condition of a corroded cable.

Since the stainless steel was used as the material for the outer conductor, the corrosion took place only within the copper coating layer atop the outer conductor. This means that immediately after the coating layer is completely corroded away, the sensor becomes corrosion insensitive. During the test of other cables, the connectors were loosened. No data was taken from the other cables.

6.5.2. The Second Test Series. To avoid the loose connector problem, all sensors were placed in the specially prepared casings as shown in Figure 6.3. These casings kept the sensors remain still during the test and data acquisition.

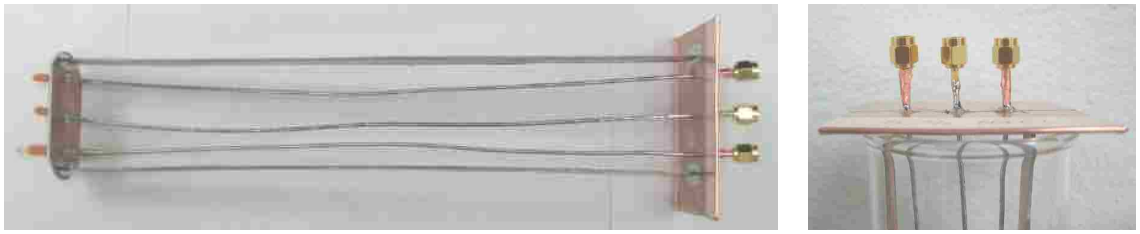

Figure 6.3. Crack/corrosion sensors encased into rigid frame to prevent connector loosening and sensor bending

Since the sensors were prepared manually, there is a possibility of embedded defects, such as zones of poorly soldered spiral edges of the outer conductor. That may lead to the solution ingress into the space between the conductor and the dielectric of a sensor at the beginning of the experiment, which can alter the electrical characteristics of the sensor. To eliminate this potential effect, three sensors were placed into distilled water. The other three sensors were placed into 3%NaCl solution. For the accelerated reaction, the remaining three sensors were submerged into 5%NaCl solution.

For various measurements, the VNA-E5071C (100 kHz-8.5GHz) was utilized during tests. The reflection coefficient (ρ) as a function of time (ns) was taken in the time domain mode. For normalization, the waveform acquired at the moment when the sensors were immersed is subtracted from each of the followed measurements. Figure 6.4 and Figure 6.5 present the normalized reflection coefficient and corrosion information of two sensors that were placed into 3% and 5% NaCl solutions, respectively. Note that the cables significantly below the air/solution interface were not corroded due mainly to lack of oxygen. Therefore, that part of the cables is not shown in Figures 6.4 and 6.5.

As shown in Figures 6.4 and 6.5, the corrosion of the cable can be divided into three zones in terms of corrosion rates.

I. Immediately below the air/solution (A/S) interface

This portion of the sensor underwent the most vigorous corrosion. The yellowish residue caused by corrosion can be seen throughout this zone. Well-developed corrosion pits can be observed on the surface of the sensors placed into the 5%NaCl solution.

II. Immediately above the air/solution (A/S) interface - intense capillary action

Capillary forces drag the corrosive solution above the A/S interface, thus oxidizing the beryllium plated cupper. The more intense supply of oxygen contributes to the process of corrosion. Due to water evaporation, salt crystals precipitate on the surface of the cable.

III. Further above the air/solution (A/S) interface - weak capillary action

With the increasing distance from the A/S interface, the attractive forces between water molecules become weaker and the amount of solution dragged upward decreases. Nevertheless a small amount of NaCl solution still reaches that zone. As the solution moves up, the salt concentration increases while the water evaporates. Accordingly, the precipitation in this zone takes place more rapidly than the corrosion process.

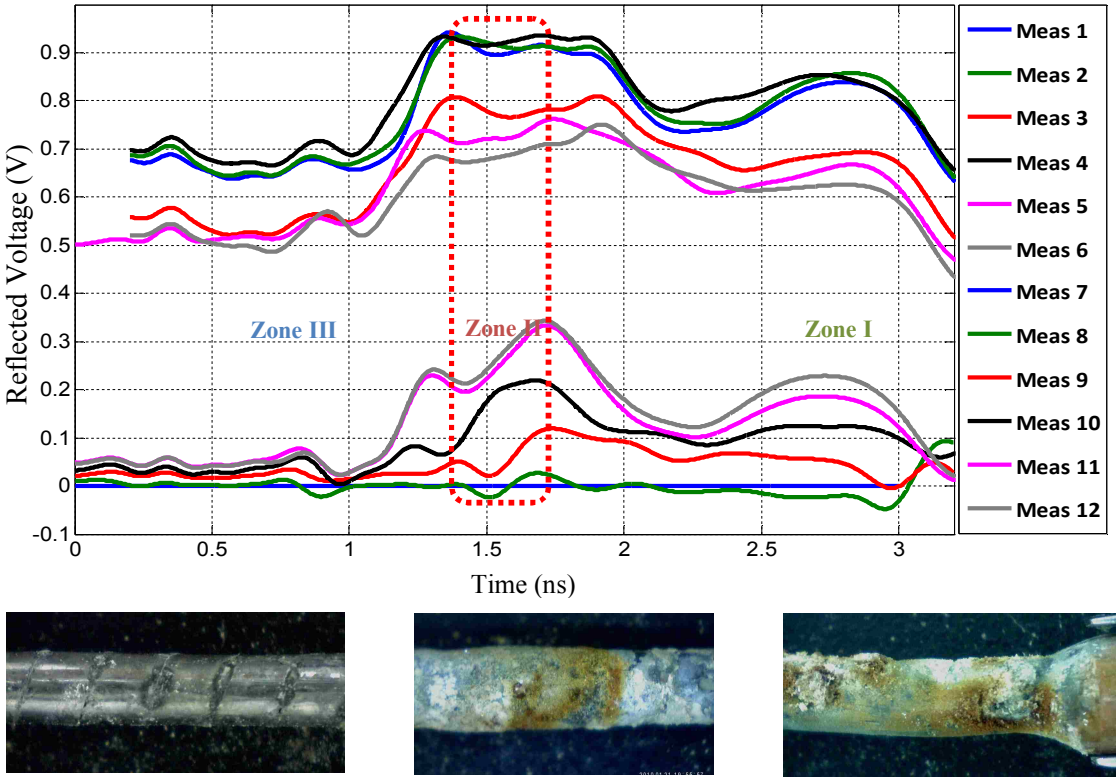

Figure 6.4. Normalized signatures and images of the sensor placed into 3% NaCl solution

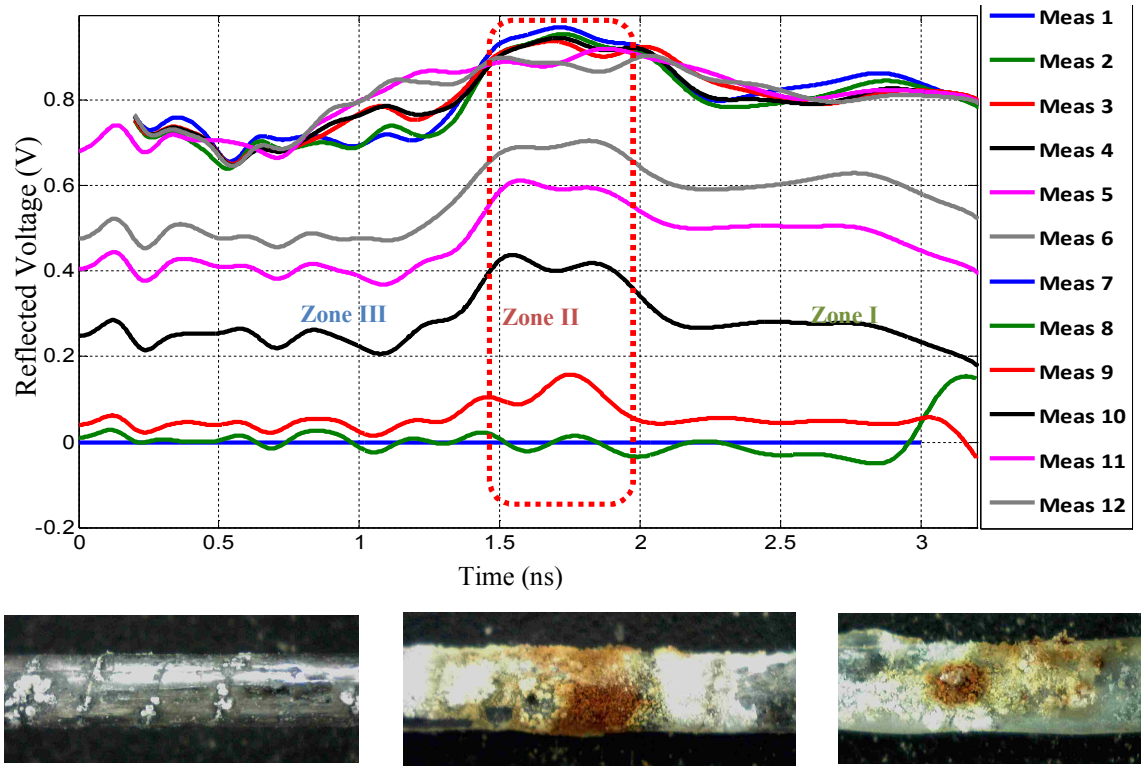

Figure 6.5. Normalized signatures and images of the sensor placed into 5% NaCl solution

Figure 6.4 indicates that the characteristic impedance of the sensor tends to increase over time. One of the reasons for this phenomenon is due to the constantly degrading condition of the outer conductor. Corrosion together with the salt precipitation along the spiral edges introduces an additional inductance, thus increasing impedance gradually. In Zone I, the corrosion process dominates this phenomenon. The outer conductor starts to corrode from the coil edges, causing the spiral separation. The sensors were hand manufactured; some degrees of imperfection are likely present. Solder used to provide electrical connectivity between spiral edges of the outer conductor may be unevenly applied, causing non uniform corrosion along the submerged portion of the cable. Therefore, several pulses can be seen in the reflection coefficient readings.

As indicated in Figure 6.5, the more aggressive environment (5% NaCl) resulted in the formation of a relatively large (to the cable's size) corrosion pit toward the end of the sensor. This possibly changed from the originally open termination to a different condition of the sensor. As conductive moisture seeps into the end of the cable, it creates gradually increasing load at the sensor's end. That can explain the rapidly drifting up signatures in Figure 6.5. The second possible explanation is the increasing losses due to water ingress into the cable. The third possible explanation is the gradually increasing inductance as salt precipitations at spiral edges of the sensor slowly push the spirals apart.

Figure 6.6 presents the normalized reflection coefficients of the sensor placed into distilled water that were measured during the corrosion tests.

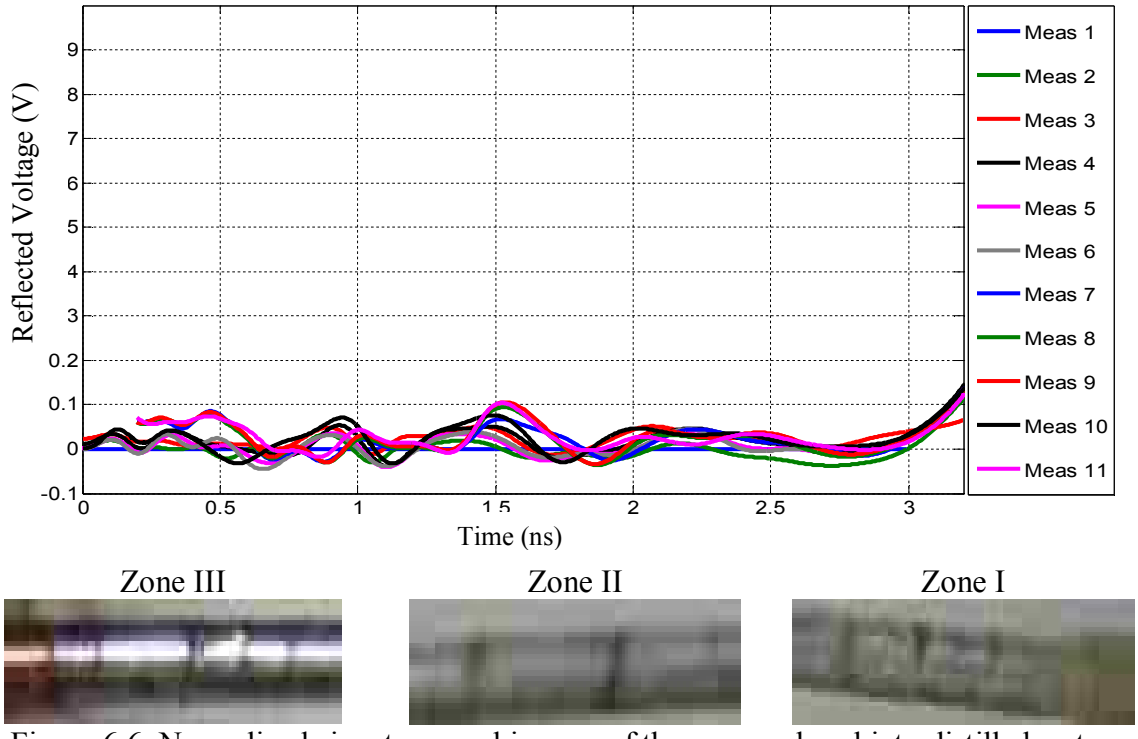

Figure 6.6. Normalized signatures and images of the sensor placed into distilled water

As one can see, the changes in the ETDR signatures are small and negligible. These results confirm that the impedance change indicated by Figures 6.4 and 6.5 is caused by the corrosion and salt precipitation processes instead of water ingress underneath the outer conductor. The end conditions of the cable did not undergo any changes during the experiment.

6.6. FORENSIC STUDY

In this study it was hypothesized that the impedance gradual increase is caused by two reasons. One is the relatively uniform separation between spiral edges caused by salt crystal precipitations. The other is the appearing of corrosion pits on the outer conductor. To validate the hypothesis, the tested sensors were disassembled and their outer conductors were carefully scrutinized under microscope (AVEN Digital Mighty Scope 1.3M). Figure 6.7 presents the condition of the outer conductors of several cables after the completion of corrosion tests.

It can be seen from Figure 6.7 that the outer conductor became thinner uniformly and more brittle during the tests. In Zone I, the presence of small (less than a millimeter) holes was evidenced. These observations validate the previous hypothesis.

The corrosion experiment indicates that the sensor can be used to locate the areas weakened by oxidation processes when embedded in steel reinforced structures. To simplify the data interpretation, the unwanted effects caused by separation of the spiral edges as a result of salt crystal precipitations can be eliminated by replacing spirally wrapped outer conductor with cylindrical copper outer conductor as shown in Figure 6.8.

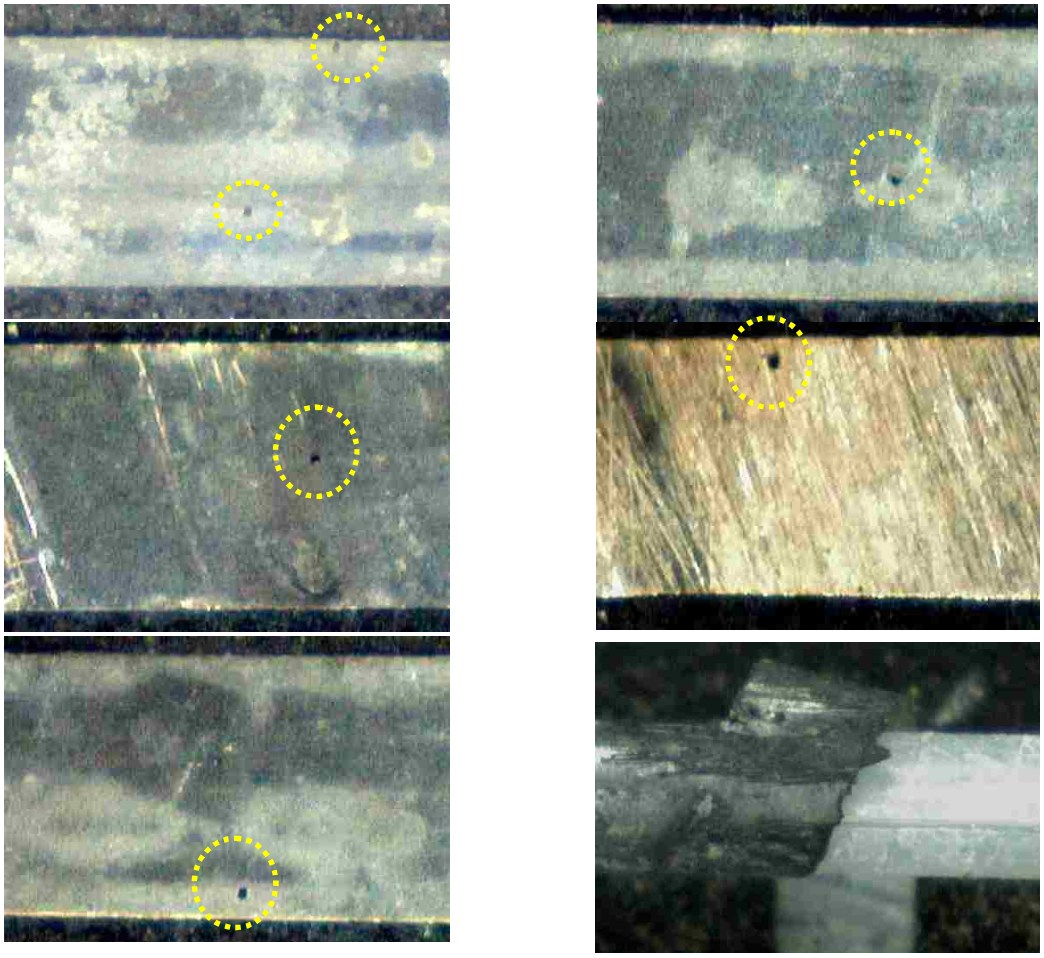

Figure 6.7. Outer conductor condition after a corrosion test

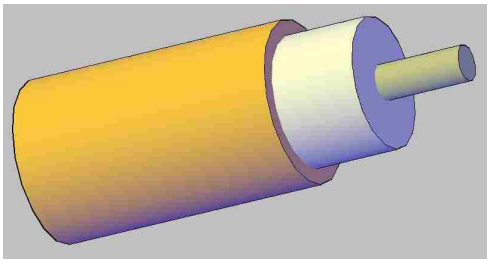

Figure 6.8. Proposed cable structure for corrosion monitoring

For practical applications, corrosion sensors must be durable and functional throughout the design life span of civil engineering structures. The signal propagation in a coaxial

cable can be interrupted when corrosion develops radially around the cable sensor surface. In this case, the cable can no longer be used as a transmitting device for further monitoring of corrosion processes. To overcome this issue, each sensor was helically covered with corrosion resistant paints as illustrated in Figure 6.9. In this way, the painted portion of the cable expects to maintain its conductive characteristics for the duration of in-service structural members, allowing continuous corrosion monitoring.

Figure 6.9. Corrosion resistant helical paints over a coaxial cable sensor

To validate the performance of corrosion sensors in application environments, 27 prototype corrosion sensors as shown in Figure 6.9 were fabricated and installed in proximity and parallel with steel reinforcement of 27 RC beams. The beams were placed in a salty sand bath and exposed to an accelerated corrosion environment. Each sensor will be used to monitor the corrosion process of its nearby parallel rebar with the VNA for the duration of corrosion tests. Finally, at the completion of the corrosion tests, each beam will be broken and the steel bars will be inspected for the location of corrosion pits. The visual inspection results will be compared with the data obtained from the sensors to draw conclusions on the sensor performance.

7. CONCLUDING REMARKS

The first part of this thesis is aimed at developing a miniaturized crack sensor with a controllable manufacturing process of coaxial cables, whose diameter is as small as one half of the previous prototype sensors. In comparison with the previous prototype, experimental data indicated that the miniaturized sensor has higher sensitivity and spatial resolution to the stress distribution and the localization of cracks. For effective deployments, both installation methods and adhesive materials were investigated for reinforced concrete applications. A surface attached crack sensor can detect cracks earlier than a corresponding embedded sensor in a RC member. It is also easier to install without the need of cutting a groove in field applications. For surface attachment of sensors, it is recommended that SikaGrout 212 be used as adhesive materials. For embedment of sensors, mortar is recommended as bonding agents.

The second portion of this thesis is a first attempt to use crack sensors for corrosion monitoring. The preliminary results obtained in this study indicated that coaxial cables function as promising distributed corrosion sensors for real time assessment of both aging and new RC structures. However, further tests and validations of corrosion sensors are required prior to actual implementation of the proposed technology.

APPENDIX A.

DATA AND RESULTS FROM THREE-POINT BENDING TEST

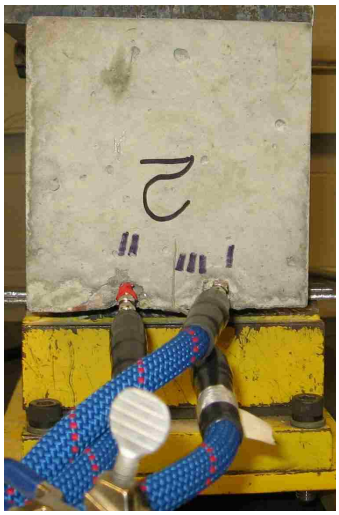

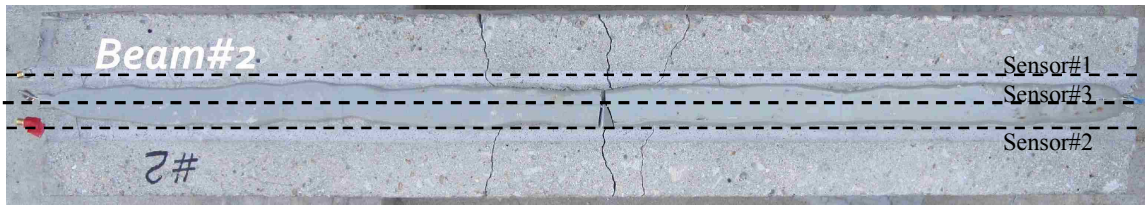

Figure A.1. Beam # 2_ PC -primer pretreated _ Hold Tight ® 102

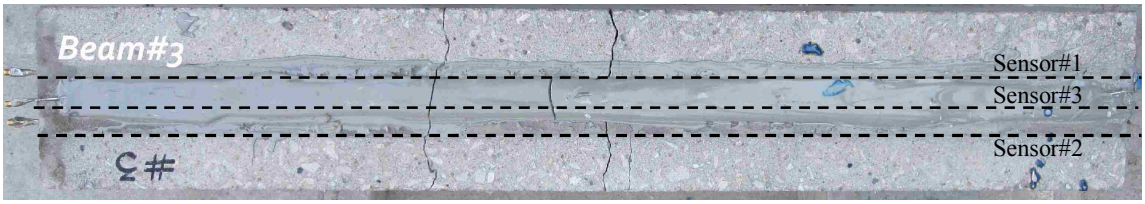

Figure A.2. Beam # 3_ Sika Grout 212_ Hold Tight ® 102

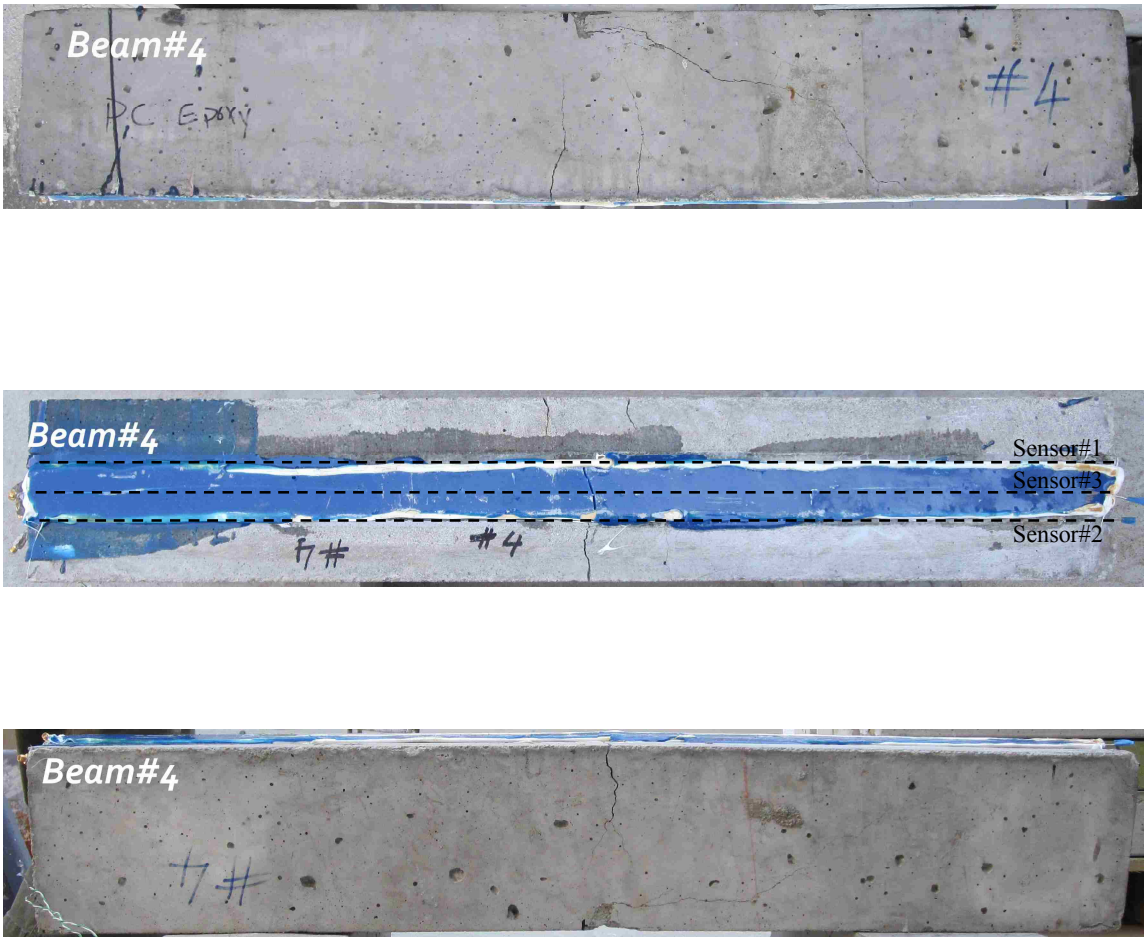

Figure A.3. Beam#4_ PC- Primer Pretreated _ Structural Epoxy

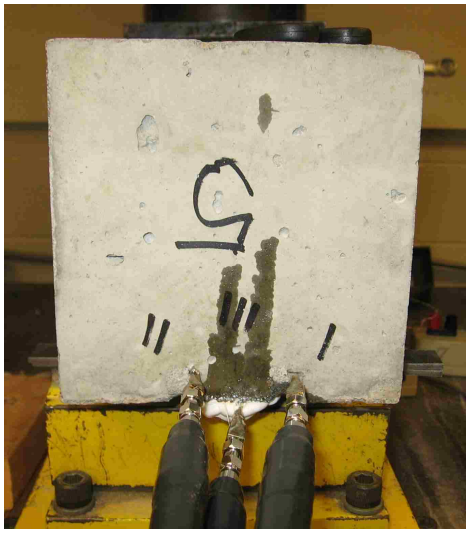

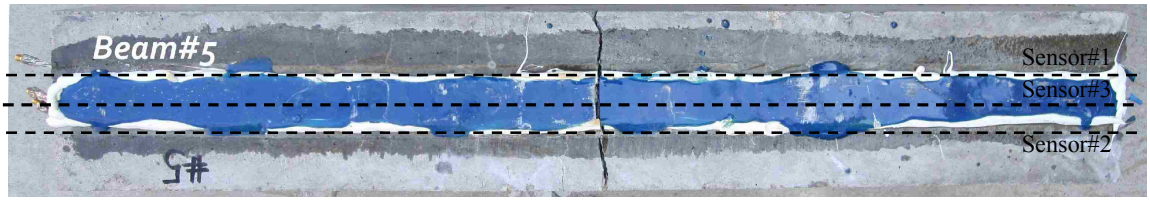

Figure A.4. Beam#5_ PC (mortar) _ Structural Epoxy

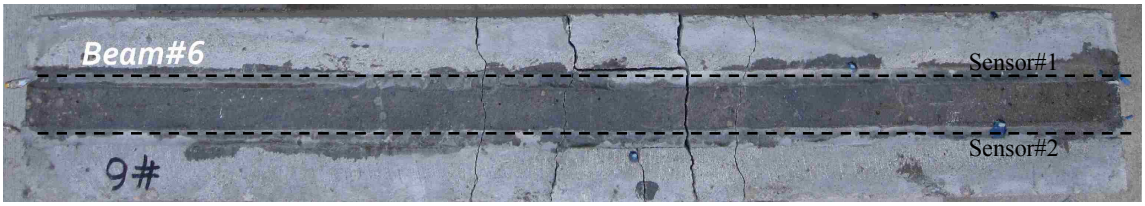

Figure A.5. Beam#6_ PC (mortar)_ none

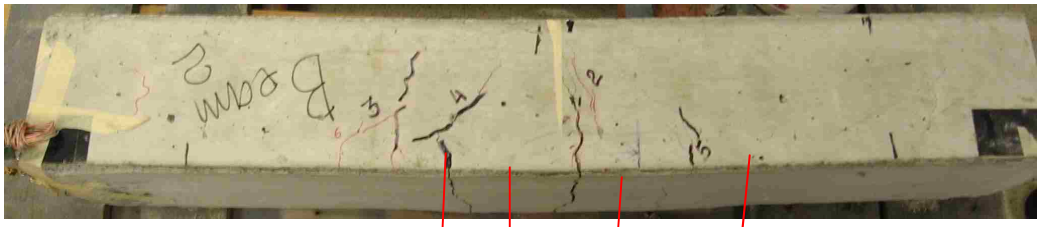

Sensor 2 (embedded) PC (mortar)

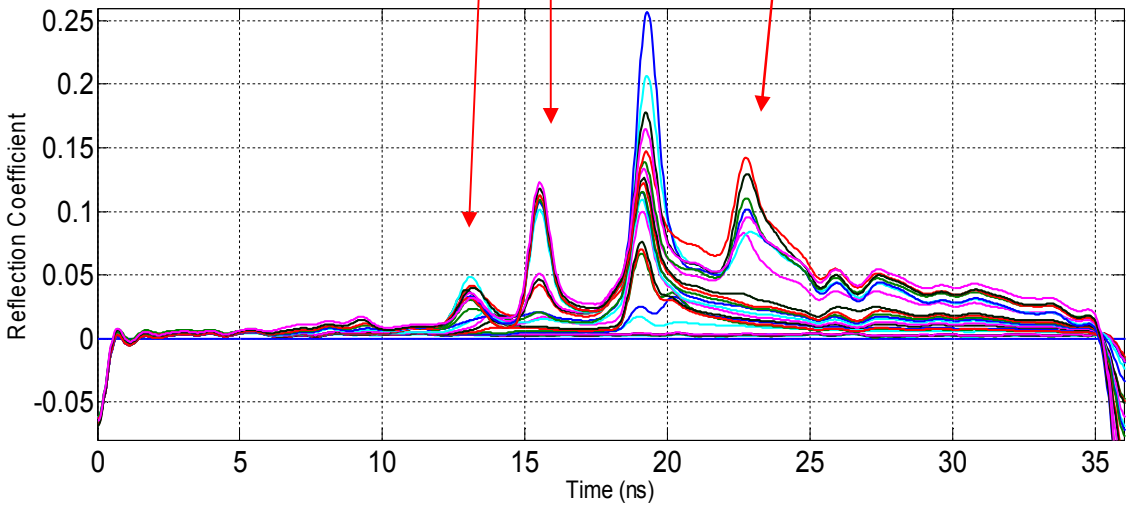

Sensor 3 (Surface Mounted) SikaGrout212

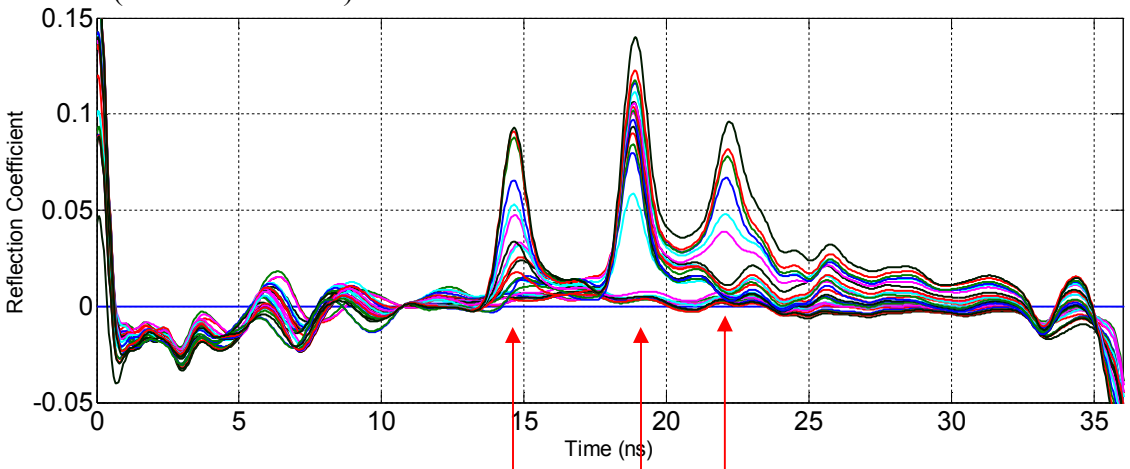

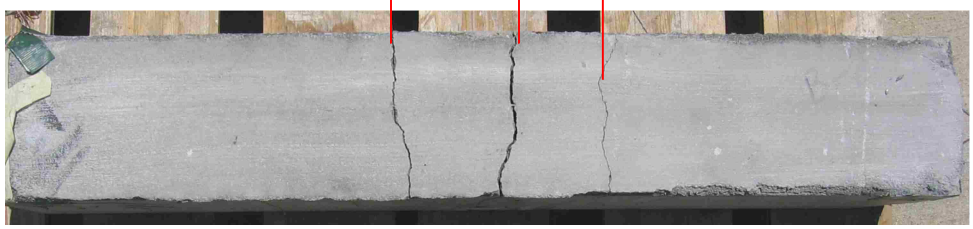

Figure A.7. Beam#8_ PC (mortar)_ SikaGrout 212

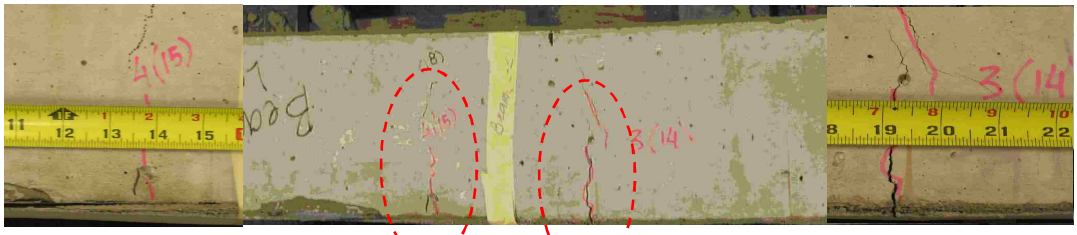

Sensor-2 (Embedded)

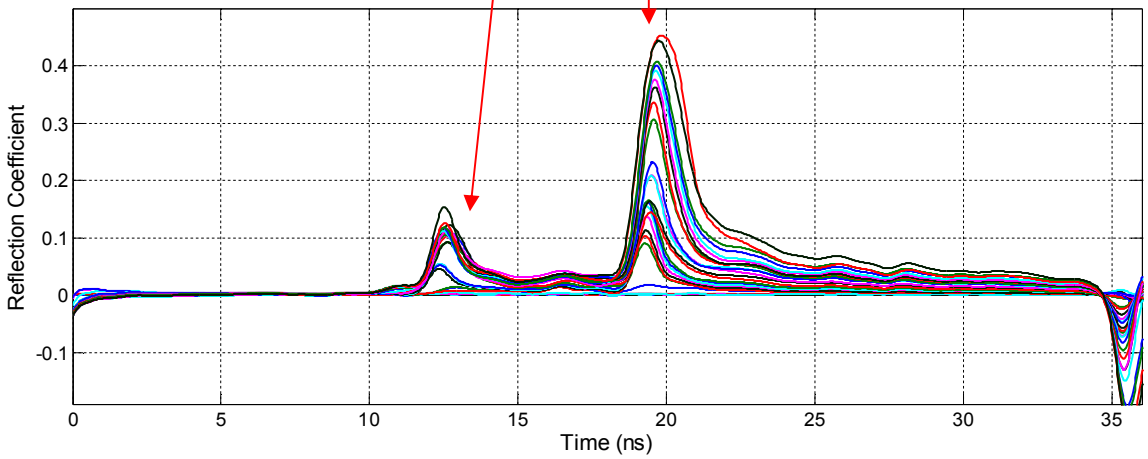

Sensor-3 (Surface Mounted)

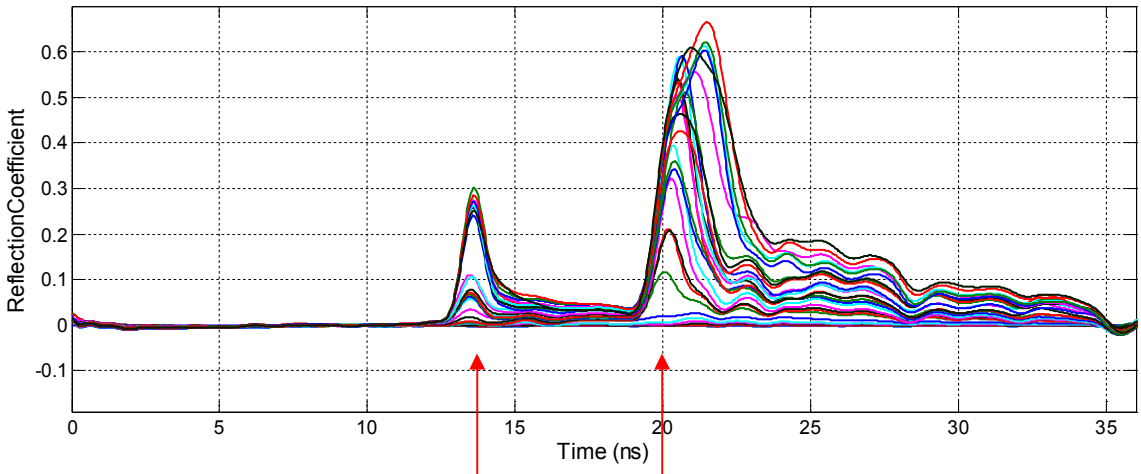

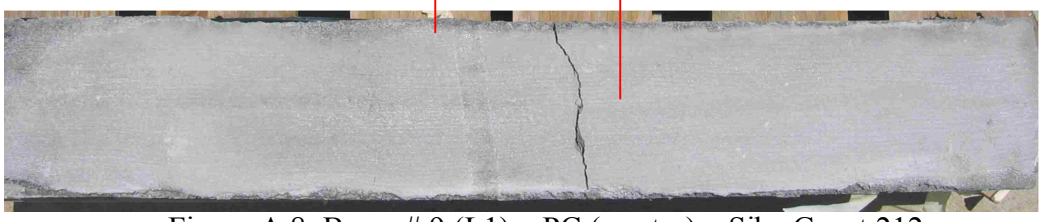

Figure A.8. Beam # 9 (L1) _ PC (mortar) _ Sika Grout 212

APENDIX B.

GEOMETRICAL MODEL AND SIMULATIONS OF CRACK SENSORS

8. B.1. SIMULATIONS

B.1.1. GENERAL CONCEPT

To perform a comprehensive optimization of coaxial cable sensors for various applications, accurate and realistic simulations of a coaxial cable is necessary. With a high fidelity model, the parameters of a cable sensor can be tested numerically to further the understanding of its behavior under different conditions. Simulation results can replace part of the time consuming and expensive experiments.

Figure B.1 presents a flow chart with three main steps to simulate the time-domain response of a cable sensor. First, a geometrical representation of the sensor (a model) is created. Since direct time-domain calculations are very time consuming, a full wave frequency domain method is used to get S-parameters. Scattering parameters or S-parameters (the elements of a scattering matrix or S-matrix) describe the electrical behaviors of linear electrical networks under various steady state stimuli by electrical signals. An equivalent circuit is then generated for the lumped element ADS model to get the time-domain response of the cable. For full-wave simulations, an electromagnetic simulation package, EMCoS Virtual Antenna Lab (EMCoS Ltd., EMCoS Antenna VirtualLab, Version 1.0), was used.

The model is represented by a spiral wrapped around a center rode on a certain distance. The loops of the spiral have small gaps between them. The surface of a spiral is created by the triangles with common edges. The return current in the model can flow from one triangle to another across the mutual edge and it cannot jump from one spiral to another. In order to create a model with connected loops, the loops across the gaps are connected by conductive segments.

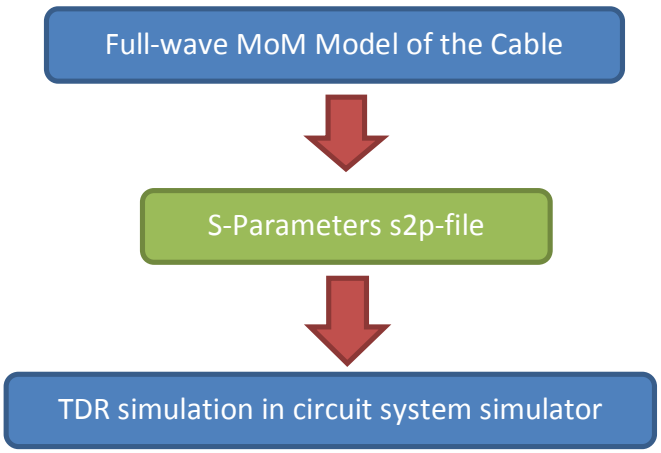

Figure B.1. Simulation flow chart

Current can flow in both triangles in the spiral and through the rods. When all gaps are connected by segments (rods), the structure behaves as a coaxial cable with a solid outer conductor. A gap in the outer conductor can be simulated by removing some rods between spirals, as illustrated in Figure B.2.

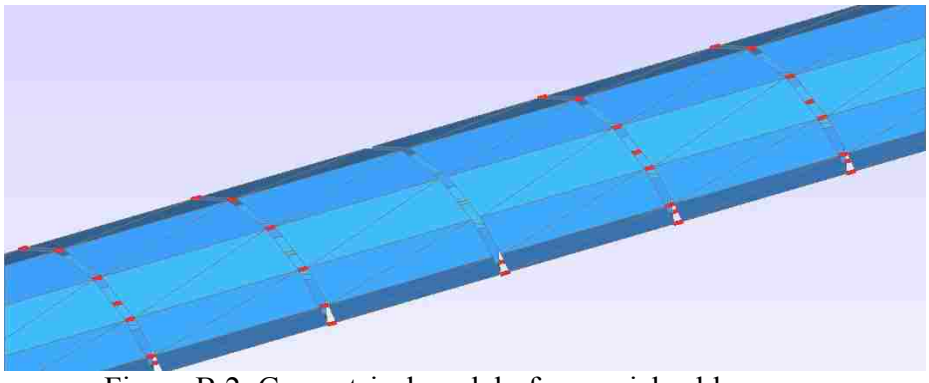

Figure B.2. Geometrical model of a coaxial cable sensor

A source is attached from one end of the cable structure (Figure B.3) and a 50 Ohm load is attached from the other end (Figure B.4). The complete model of the cable is shown in Figure B.5.

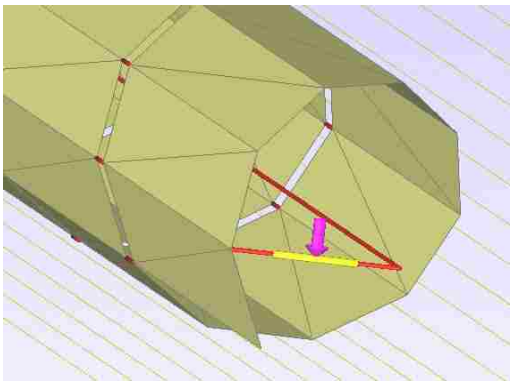

Figure B.3. Source simulation

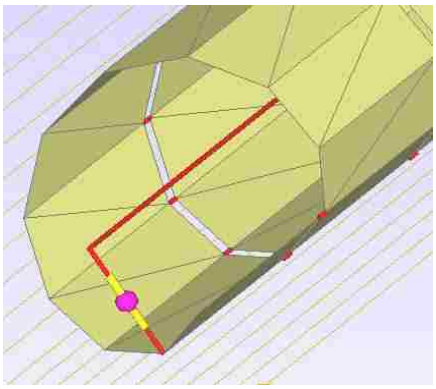

Figure B.4. Termination simulation

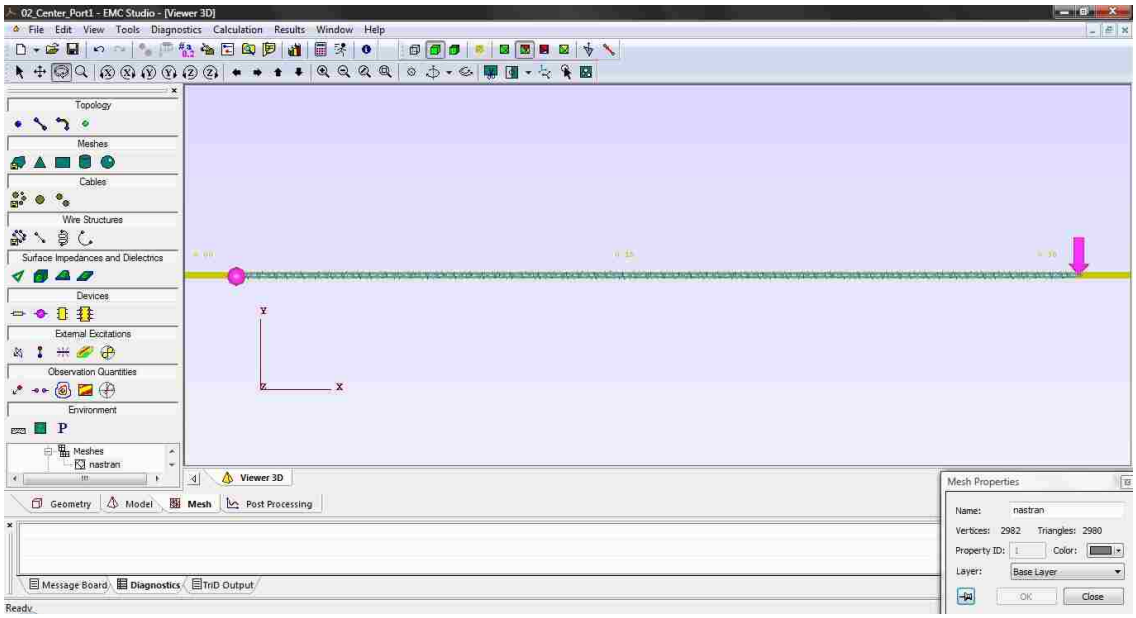

Figure B.5. The complete model of a coaxial cable sensor in EMC Studio

Surface current distribution for 1 MHz frequency is presented in Figure B.6. Effect of discontinuity can be clearly seen. Red color represents high current density.

Current Distribution Arrow Plot can be used to visualize the current flow direction as shown in Figure B.7.

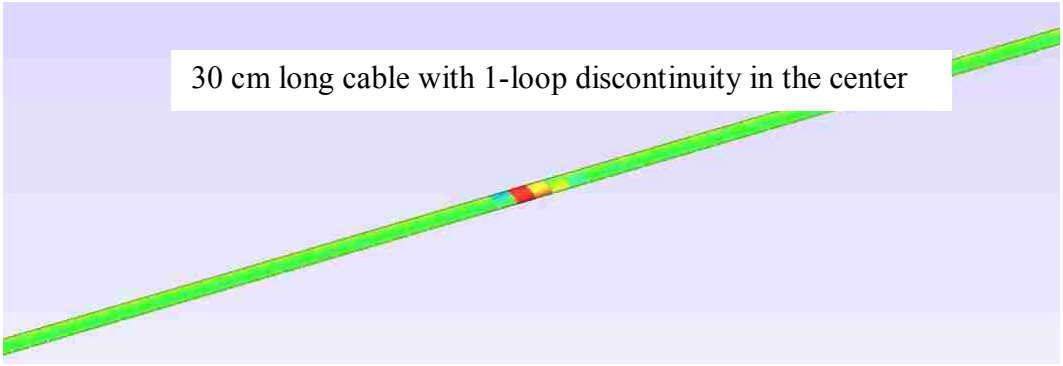

Figure B.6. Current distribution across the gap

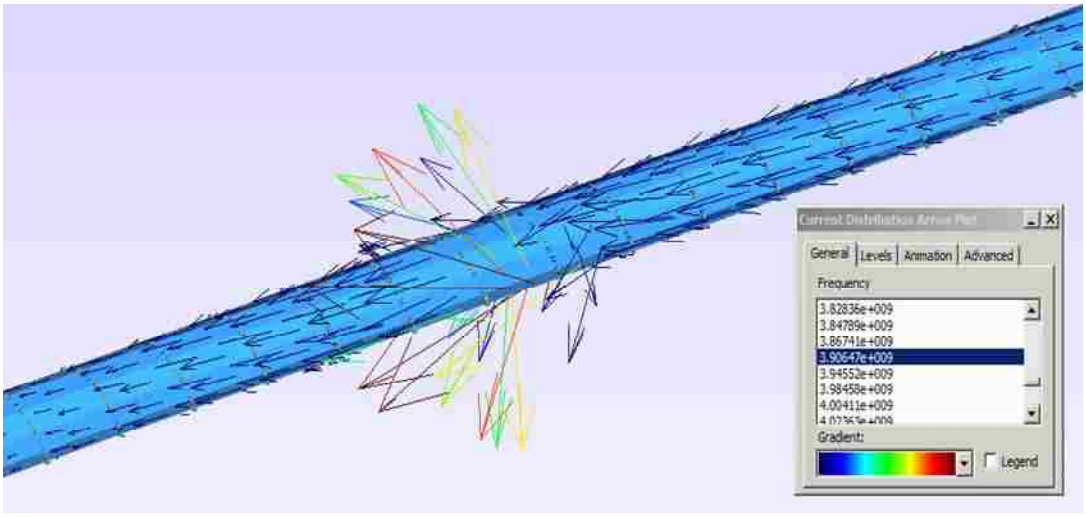

Figure B.7. Current Distribution Arrow Plot

In the normal state of a cable when loops are connected with conductive elements, current flows along the cable. In case of discontinuity, current is forced to take detour by spiral shield. This affects S-parameters of the cable as illustrated in Figure B.8 – B.10.

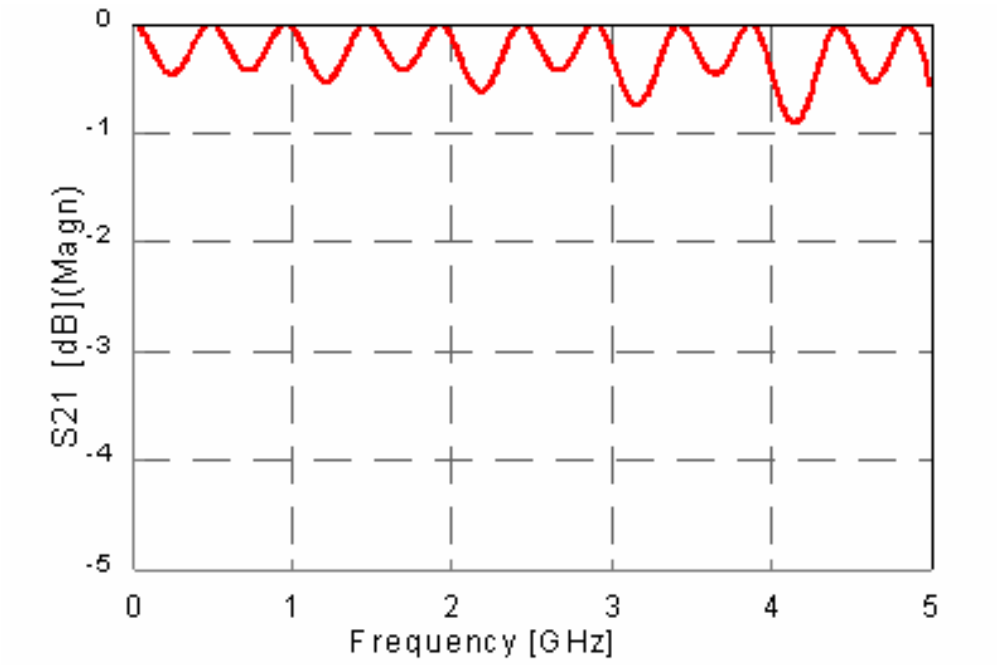

Figure B.8. Transmission coefficient

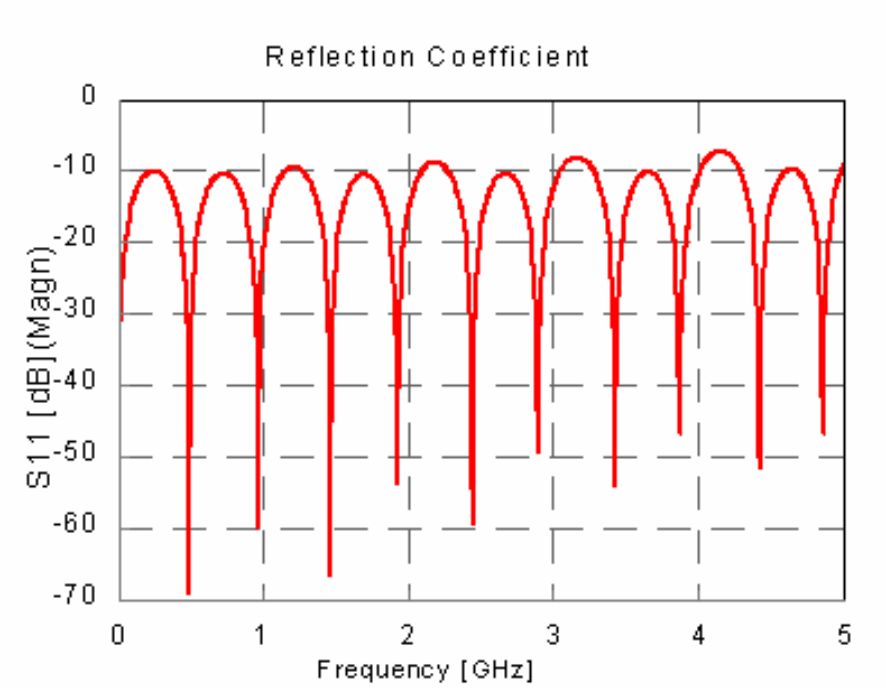

Figure B.9. Reflection coefficient

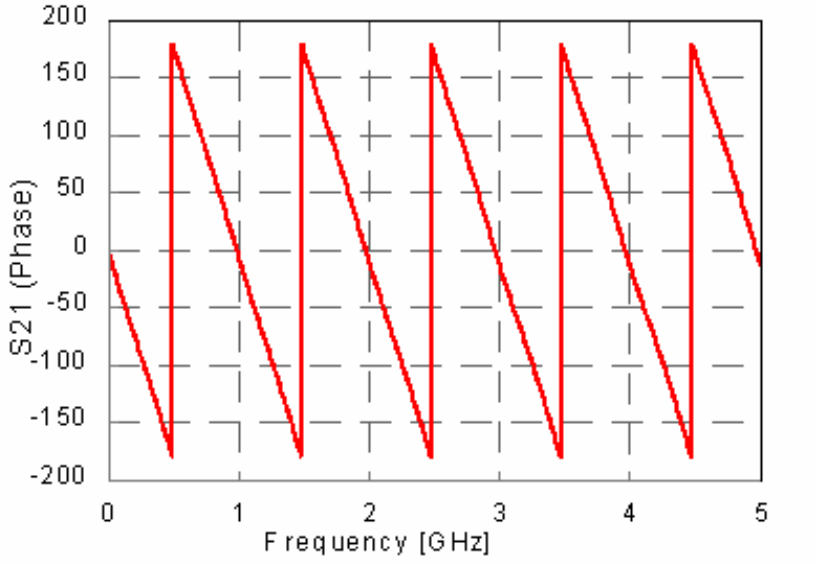

Figure B.10. Transmission coefficient

Therefore, any change in S-parameters matrix is detectable in TDR simulations using the ADS model as shown in Figure B.11. The model assumes that the source (TDR) has a rise time of 34 ps. TDR is connected to the block created based on the simulated S-parameters via 50 Ohm impedance.

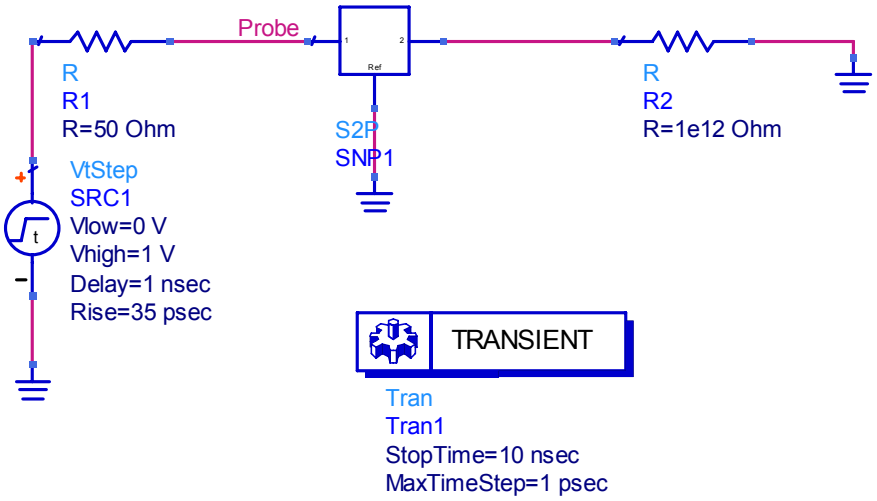

Figure B.11. ADS model of the setup with TDR and the sensor

As shown in Figure B.12 for the TDR simulations, the peak that represents the gap in the cable is not well distinguishable. There are following reasons and ways to improve the simulation. The main reason is that the full wave simulation uses a frequency range up to 5 GHz. The wavelength at 5 GHz is around 15 cm. This means that much higher frequencies must be used to “feel” the gap.

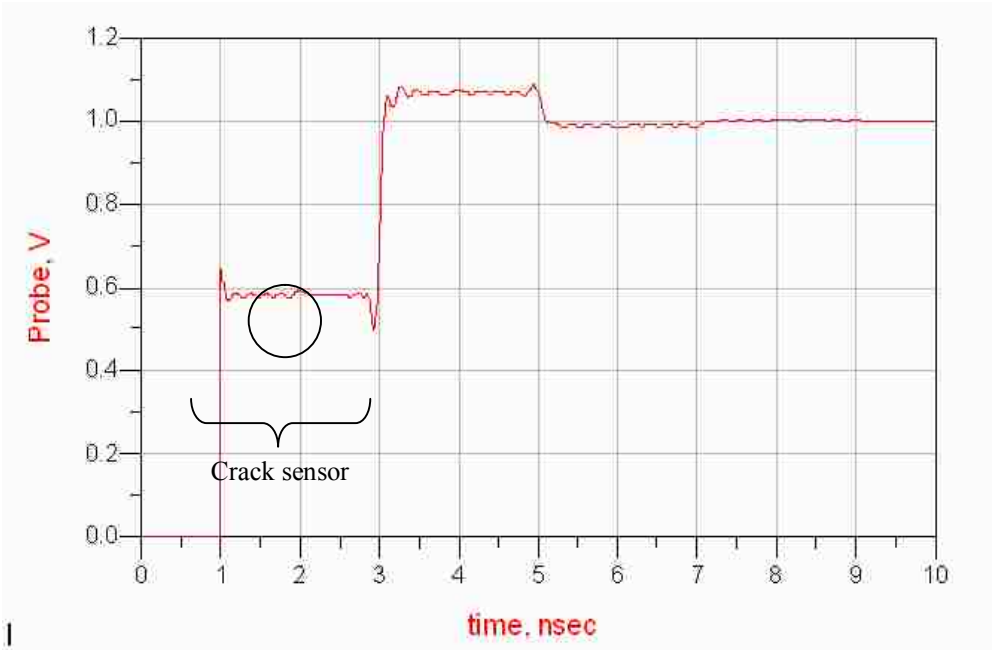

Figure B.12. TDR simulations with ADS

APPENDIX C.

GEOMETRICAL MODEL GENERATION CODE IN C#

```
namespace NastranCableGenerator
{
   public partial class Form1 : Form
   {
      public Form1()
      {
         InitializeComponent();
      }

      private void buttonGenerate_Click(object sender, EventArgs e)
      {
         GenerateSpiral();
         return;
         double cable_length;
         double cable_diameter;
         double spiral_pitch;
         double spiral_width;
         int circular_approximation;

         cable_length = Convert.ToDouble(textBoxLength.Text);
         cable_diameter = Convert.ToDouble(textBoxDiameter.Text);
         spiral_pitch = Convert.ToDouble(textBoxPitch.Text);
         spiral_width = Convert.ToDouble(textBoxWidth.Text);
         circular_approximation = Convert.ToInt32(textBoxApproximation.Text);

         double pitch_angle;
         pitch_angle = Math.Tan((spiral_pitch / 2.0) / cable_diameter);
         //pitch_angle = pitch_angle * 180.0 / Math.PI;
         double width_along_cable;
         width_along_cable = spiral_width / Math.Cos(pitch_angle);

         double step_angle = 360.00/Convert.ToDouble(circular_approximation);
         step_angle = step_angle / 180.0 * Math.PI;

         //Prepare to create Spiral.

         double NumberOfTurnes = cable_length / spiral_pitch;
```

```
        int NumberOfSteps = Convert.ToInt32(NumberOfTurnes *
Convert.ToDouble(circular_approximation));
        double StepSize = cable_length / NumberOfSteps;

        Vector3D Vector_1, Vector_X;

        Vector_1.X = 0.0;
        Vector_1.Y = 0.0;
        Vector_1.Z = cable_diameter/2.0;

        Vector_X.X = 1.0;
        Vector_X.Y = 0.0;
        Vector_X.Z = 0.0;

        List<Vector3D> Pos = new List<Vector3D>();

        for (int i = 0; i <= NumberOfSteps; i++)
        {

            Vector_1 = Vector3D.RotateVectorAroundVector(Vector_X, Vector_1,
step_angle*Convert.ToDouble(i));
            Vector3D tmpVector = Vector_1;
            tmpVector.X = StepSize*Convert.ToDouble(i);
            Pos.Add(tmpVector);

            tmpVector.X = StepSize * Convert.ToDouble(i) + width_along_cable;
            Pos.Add(tmpVector);

        }


            TextWriter tw = new StreamWriter("nastran.nas");
            string ToWrite;

            for(int i = 0; i < Pos.Count; i++)
            {
              //cable_diameter.ToString();
```

```
            ToWrite = CreateNode(i+1, Pos[i].X, Pos[i].Y, Pos[i].Z);

            tw.Write(ToWrite);
        }

        for (int i = 0; i < Pos.Count - circular_approximation; i += circular_approximation)
        {

            for (int j = 0; j < circular_approximation-1; j+=2)
            {
                ToWrite = CreateTriangle(j + i + 1, j + i + 1, j + i + 3, j + i + 2); //1 3 2
                tw.Write(ToWrite);

                ToWrite = CreateTriangle(j + i + 2, j + i + 2, j + i + 3, j + i + 4); //2 3 4
                tw.Write(ToWrite);
            }

            ToWrite = CreateTriangle(i + circular_approximation - 1, i + circular_approximation - 1, i +
1, i + circular_approximation * 2); //2 3 4
            tw.Write(ToWrite);

            ToWrite = CreateTriangle(i + circular_approximation , i + circular_approximation, i + 1, i +
2); //2 3 4
            tw.Write(ToWrite);

        }

        //ToWrite = CreateTriangle(1234, 123, 1, 23);

        tw.Write("ENDDATA");

       tw.Close();

    }

    private string CreateNode(int id, double X, double Y, double Z)
```

```
{
        string nX = String.Format("{0,7:0.00}", X);// X.ToString("G6");
        string nY = String.Format("{0,7:0.00}", Y);//Y.ToString("G6");
        string nZ = String.Format("{0,7:0.00}", Z);//Z.ToString("G6");

        string s_id;// = id.ToString();

        //GRID          1       0 0.55352 0.69243  0.8866

       s_id = String.Format("{0,5}", id);

   string signX = " ", signY = " ", signZ = " ";

   string res_string;

   res_string = "GRID       " + s_id + "       0" + signX + nX  + signY + nY  + signZ + nZ + "\n";

   return res_string;

}

private string CreateTriangle(int id, int n1, double n2, double n3)
{

   //CTRIA3        1     200      4     13     147

   string res_string;

   string s_id = String.Format("{0,5}", id);

   res_string = "CTRIA3     " + s_id + "     200" + String.Format("{0,8}", n1) +
                        String.Format("{0,8}", n2) + String.Format("{0,8}", n3) + "\n";

   return res_string;
}

void GenerateSpiral()
```

```
{
    double cable_length = Convert.ToDouble(textBoxLength.Text);
    double cable_diameter = Convert.ToDouble(textBoxDiameter.Text);
    double spiral_pitch = Convert.ToDouble(textBoxPitch.Text);
    double spiral_width = Convert.ToDouble(textBoxWidth.Text);
    double circular_approximation = Convert.ToInt32(textBoxApproximation.Text);

    Vector3D axe = new Vector3D(1.0, 0.0, 0.0);
    Vector3D vec = new Vector3D(0.0, 0.0, cable_diameter / 2.0);

    List<Vector3D> spiral1 = new List<Vector3D>();
    List<Vector3D> spiral2 = new List<Vector3D>();

    double step = spiral_pitch / circular_approximation;

    step = cable_length/Math.Round(cable_length / step);

    double angle = Math.PI * 2.0 * (step / spiral_pitch);

    double N = Math.Floor(cable_length - spiral_width) / step;
    Vector3D origin = new Vector3D(0.0, 0.0, 0.0);
    for (int i=0;i<=N;i++)
    {
        vec = Vector3D.RotateVectorAroundVector(axe, vec, angle);
        spiral1.Add(origin + vec);
        spiral2.Add(origin + vec + (new Vector3D(spiral_width, 0, 0)));
        origin.X += step;
    }

    TextWriter tw = new StreamWriter("nastran.nas");
    string ToWrite;
    int n = 0;
    for (int i = 0; i < spiral1.Count; i++)
    {
        //cable_diameter.ToString();

        ToWrite = CreateNode(++n, spiral1[i].X, spiral1[i].Y, spiral1[i].Z);
```

```
            tw.Write(ToWrite);
        }

        for (int i = 0; i < spiral2.Count; i++)
        {
            //cable_diameter.ToString();

            ToWrite = CreateNode(++n, spiral2[i].X, spiral2[i].Y, spiral2[i].Z);

            tw.Write(ToWrite);
        }

        n = 0;
        for (int i = 0; i < spiral1.Count-1; i++ )
        {
            ToWrite = CreateTriangle(++n,i+1,i+2,i+spiral1.Count+1); //1 3 2
            tw.Write(ToWrite);

            ToWrite = CreateTriangle(++n, i + 2, i + spiral1.Count + 2, i + spiral1.Count + 1); //2 3 4
            tw.Write(ToWrite);
        }

        int nTurns = (int) Math.Floor(cable_length / spiral_pitch);
        n = 0;
        for (int i = 0; i < spiral1.Count - (int)circular_approximation; i++)
        {
            ToWrite = CreateRod(++n, i + spiral1.Count + 1, i + (int)circular_approximation+1);
            tw.Write(ToWrite);
        }

        tw.Close();
    }

    private string CreateRod(int id, int n1, int n2)
    {
        //CROD         1       1     926     929
```

```
            string res_string;

            string s_id = String.Format("{0,5}", id);

            res_string = "CROD       " + s_id + "       1" + String.Format("{0,8}", n1) +
                                 String.Format("{0,8}", n2) + "\n";

            return res_string;
        }
};

}
```

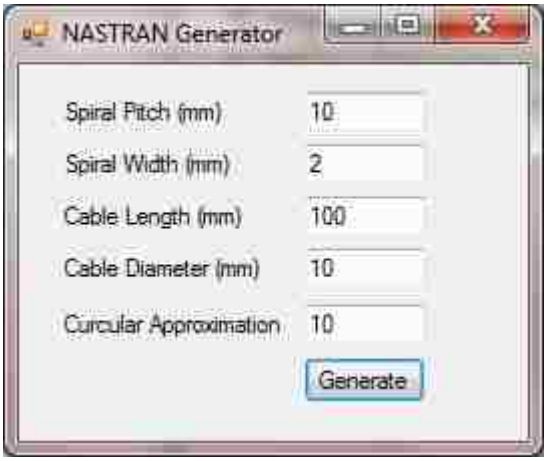

BIBLIOGRAPHY

Brower, M. A., Implementation issues of distributed coaxial cable crack sensors embedded in reinforced concrete members, M.S. Thesis, University of Missouri-Rolla, Rolla, MO, 2007.

Brower, M. A., Royer, Z. L., Chen, G. D., Van Aken, D. C., Pommerenke, D., Distributed Cable Sensors for Structural Damage Detection: Implementation Issues, Proceedings of the 2006 ASCE Structural Congress, St. Louis, May 18-20, 2006.

Cerri, G., De Leo, R., Della Nebia, L., Pennesi, S., Primiani, V. M., and Russo, P., Fault location on shielded cables: Electromagnetic modeling and improved measurement data processing, IEE, 2005.

Chen, G. D., Sun, S. S., Pommerenke, D., Drewniak, J. L., Greene, G. G., McDaniel, R. D., Belarbi, A., and Mu, H. M., Crack detection of a 15 meter long reinforced concrete girder with a single distributed cable sensor, Proceedings of 1st International Conference on Structural Health Monitoring and Intelligent Infrastructures, Tokyo, Japan, November 2003.

Chen, G. D., Development and validation of novel distributed coaxial cable sensors for crack detection, Proceedings of 3rd Sino-Japan-US Symposium on Structural Health Monitoring and Control, Dalian, China, October 2004.

Chen, G. D., Mu, H., Pommerenke, D., and Drewniak, J. L., Damage detection of reinforced concrete beams with novel distributed crack/strain sensors, Struct. Health Mon., 3(3): 225-243, 2004.

Chenaf, D., and Amara, N., Time domain reflectometry for the characterization of diesel contaminated soils, Second International Symposium and Workshop on Time Domain Reflectometry, 2001.

Clayton, R. Paul, Introduction to Electromagnetic Compatibility, 1992.

Comoda, M., Kawashima, T., Arakane, M., Aihara, M., Fujiwara, Y., and Shinagawa, J., Development of a current detection type fault locator, IEEE Transactions On Power Delivery, 6, pp. 541–545, 1991.

Dalton, F. N., and Van Genuchten, M. Th., The TDR method for measuring soil water content and salinity, Northwestern University, Evanston, Illinois, 2001.

Douding, C. H., Su, M. B., and O'Connor, K., Measurements of rock mass deformation with grouted coaxial antenna cables, 1987.

Grozic, J. L., Lefebvre, M. E., Robertson, P. K., and Morgenstern, N. R., Using Time Domain Reflectometry in Triaxial Testing, 2000.

Iskander, M. F., Electromagnetic fields and waves, Prentice Hall, Englewood Cliffs, NJ, 1992.

Koch, G. H., Brongers, P. H., Thompson, N. G., Virmani, Y. P., and Payer, J. H., Corrosion Costs and Preventive Strategies in the United States, Federal Highway Administration Report FHWA-RD-01-156, 30 Sep 2001.

Lin, M. W., Abatan, A. O., and Zhang, W., Crack damage detection of concrete structures using distributed electrical time domain reflectometry (ETDR) sensors, Proceedings of 5th SPIE Annual Symposium on Smart Structures and Materials: Smart Systems for Bridges, Structures, and Highways, Vol. 3325, Newport Beach, 1998.

Lin, M. W., Abatan, A. O., and Zhou, Y., High sensitivity electric TDR distributed strain sensor, Proceedings of 7th SPIE Annual Symposium on Smart Structures and Materials 2000: Smart Systems for Bridges, Structures, and Highways, Vol. 3986, Newport Beach, March 2003.

Lin, M. W., Thaduri. J, and Abatan, A. O., Development of an electrical time domain reflectometry distributed strain sensor, 2005.

McDaniel, R. D., Characterization and implementation of distributed coaxial cable sensors for embedment in reinforced concrete structural members, M.S. Thesis, University of Missouri-Rolla, MO, 2004.

Mehran Khoshbakht, and Mark W. Lin, Development of an electrical time domain reflectometry (ETDR) distributed moisture measurement technique for porous media 2006.

Mu, H., Development and validation of coaxial cable sensors for damage detection of reinforced concrete structure, Ph.D. Dissertation, Department of Civil, Architectural, and Environmental Engineering, University of Missouri-Rolla, MO, 2002.

Nawy, E. G., Reinforced Concrete: a Fundamental Approach, 5th Edition, Prentice Hall, Upper Saddle River, NJ, 1998.

O'Connor, K. M., Murphy, E. W., TDR monitoring as a component of subsurface risk assessment over abandoned mines, 1997.

Paul Virmany, Corrosion Cost and Preventive Strategies in the United States, Publication No. FHWA-RD-01-156, Y, 2001.

Sun, S., Pommerenke, D. J., Drewniak, J. L., Chen, G., Liang Xue, Brower, M. A., and Koledinceva, M. Y., A Novel TDR-Based Coaxial Cable Sensor for Crack/Strain sensing in Reinforced Concrete Structures, 2009

Wang, M., Electromagnetic modeling of distributed coaxial cable crack sensors in reinforced concrete members, Thesis, 2008.

Yuepipng Yin, Hongbe Wang, Youlong Gao and Xiaochin Li, Real time monitoring and early warning of landslides at relocated Wushan Town, the Three Gorges Reservoir in China, 2009.

VITA

Iana Muchaidze was born in Tbilisi, Georgia. Iana graduated from high school in May of 1991from Feliks Edmundowicz Dzerzhinsky High school in Tbilisi, Georgia. She then attended the Georgian Technical University in Tbilisi, Georgia. In December of 1998, Iana received her Bachelor's of Science Degree in Civil Engineering. Following graduation, Iana was employed by military organization "Delta", Tbilisi, Georgia.

In August of 2006 Iana enrolled at the University of Missouri-Rolla and in August of 2008, she completed her Master of Science in Geological Engineering from Missouri University of Science and Technology (former University of Missouri- Rolla).

Her Master's thesis was entitled "Imaging in Karst Terrain Using Electrical Resistivity Tomography." Iana continued her studies at the Missouri University of Science and Technology, beginning her second Master of Science degree in Civil Engineering in August 2008. The following year she was inducted into Chi Epsilon, as a chapter member of the Missouri University of Science and Technology. Iana completed her Master of Science in Civil Engineering under the Center for Infrastructure Engineering Studies with the aid of a graduate research assistantship in December of 2010; her second Master's thesis was entitled "Installation and Performance Evaluation of Coaxial Cable Sensors for Crack and Corrosion Detection."